Master's Thesis

DIRECT MATERIAL PATTERNING ON CURVED SUBSTRATES USING FLEXIBLE MOLDS WITH THROUGH-HOLE AND POST ARRAYS

Youngchul Chae

Department of Mechanical Engineering

Ulsan National Institute of Science and Technology

2021

DIRECT MATERIAL PATTERNING ON CURVED SUBSTRATES USING FLEXIBLE MOLDS WITH THROUGH-HOLE AND POST ARRAYS

Youngchul Chae

Department of Mechanical Engineering

Ulsan National Institute of Science and Technology

DIRECT MATERIAL PATTERNING ON CURVED SUBSTRATES USING FLEXIBLE MOLDS WITH THROUGH-HOLE AND POST ARRAYS

A thesis/dissertation submitted to
Ulsan National Institute of Science and Technology
in partial fulfillment of the
requirements for the degree of
Master of Science

Youngchul Chae

07.15.2021 of submission

Approved by

Advisor

Taesung Kim

DIRECT MATERIAL PATTERNING ON CURVED SUBSTRATES USING FLEXIBLE MOLDS WITH THROUGH-HOLE AND POST ARRAYS

Youngchul Chae

This certifies that the thesis/dissertation of Youngchul Chae is approved.

07.15.2021 of submission

Signature

Advisor: Taesung Kim

Signature

Jaesung Jang

Signature

Hoon-Eui Jeong

Signature

ABSTRACT

Many attempts to confer mechanical robustness and flexibility on transparent conducting electrodes (TCEs) even with large deformations have been made to date because displays, solar cells, touch screens, and wearable electronics have been rapidly growing on-demand. Recently, there has been interested in low-cost, facile, and scalable patterning methods to replace conventional indium tin oxide (ITO) electrodes that have complex fabrication issues and are inflexible. Here, we present a direct material patterning method of silver-mesh flexible transparent conducting electrodes (SMFTCEs), which can maintain not only constant electrical properties but also high durability against repeated mechanical bending regardless of substrate curvatures. Using the template-guided foaming (TGF) technique, the liquid-air interfaces are gradually pushed out during liquid evaporation on curved substrates, allowing patterning within several minutes in a single step. Then, assembling silver nanowires (AgNWs) into aligned 2D foam structures enables the fabrication of curvilinear conductive grids in a high-throughput manner. We report the low sheet resistance, high transmittance, and mechanical robustness of the resulting SMFTCEs against repeated bending. We demonstrated that the SMFTCEs showed comparable optoelectronic properties, resulting in the sheet resistance of 14.87 Ω/sq at a transmittance of 80%. In addition, we characterized that their mechanical flexibility is as comparable as others literature, showing the electrical resistance change of less than 5% for repeated bending cycles of 10,000 times with a small radius of curvature of 3 mm. Furthermore, we applied the direct material patterning method to various materials. For example, we employed a polymer solution of PEDOT:PSS and then demonstrated it can be printed/patterned on curvilinear substrates in the same manner as SMFTCEs. To overcome the limitation of patterning only when the liquid completely evaporates, we also successfully fabricated liquid films that secure long-term stability using oil and non-polar organic solvents. Hence, we believe that our study could provide a novel fabrication strategy and show high potential for flexible electronics and next-generation wearable systems.

Table of Contents

List of Figures

List of Tables

Nomenclature

2D: two-dimensional

3D: three-dimensional

AgNWs: silver nanowires

CCD: charge-coupled device

CNTs: carbon nanotubes

CuNWs: copper nanowires

FE-SEM: field emission scanning electron microscope

FTCEs: flexible transparent conducting electrodes

ITO: indium tin oxide

LP: liquid patterning

OLED: organic light-emitting diodes

OSTEMER: off-stoichiometry thiol-ene polymer resin

PC: polycarbonate

PDMS: polydimethylsiloxane

PEDOT:PSS: poly(3,4-ethylenedioxythiophene)-poly(styrenesulfonate)

PET: polyethylene terephthalate

PFOCTS: trichloro(1H,1H,2H,2H-perfluorooctyl)silane

PFTCEs: polymer flexible transparent conducting electrodes

PVA: poly(vinyl alcohol)

SDS: sodium dodecyl sulfate

SMFTCEs: silver-mesh flexible transparent conducting electrodes

TCEs: transparent conducting electrodes

TGF: template-guided foaming

TMSCI: chlorotrimethylsilane

UV: ultraviolet

Ω: SI derived unit of electrical resistance

$\boldsymbol{x_n}$**:** liquid film thickness

$\boldsymbol{\gamma}$**:** surface tension

$\boldsymbol{\eta}$**:** viscosity

$\boldsymbol{h}$**:** liquid film height

$\boldsymbol{f_{evap}}$**:** evaporation rate

$\mathbf{h_p}$**:** height of the post

$\mathbf{d_p}$**:** diameter of the post

l: distance between posts

Chapter 1. Introduction

1.1 Microfluidic approaches through micro-/nanoscale patterning

Liquid has the property of deforming when force is applied from the outside. Efforts have been made to apply these liquids to microfluidics by engineering them into the desired shape[1, 2]. Recently, as the technology of micro-/nano fabrication and technology advances, researches on applying to patterning using interfaces while controlling the shape and shape of liquids are increasing[3-6]. There was a case of developing a technology to increase resolution compared to cost by combining the advantages of soft lithography, bottom-up approach, and microfluidic manipulation, and also developed a method to maximize the merits of liquid-mediated patterning by increasing both throughput and applicability[7, 8]. For example, Juyeol Bae et al. developed a membrane-assisted micro-/nanofluidic liquid-mediated patterning technology. Liquid patterning using a microfluidic device allows the evaporation of a liquid to occur naturally through micro-holes in the device and allows the evaporating liquid to be fixed to the micro-posts to form a two-dimensional film[9].

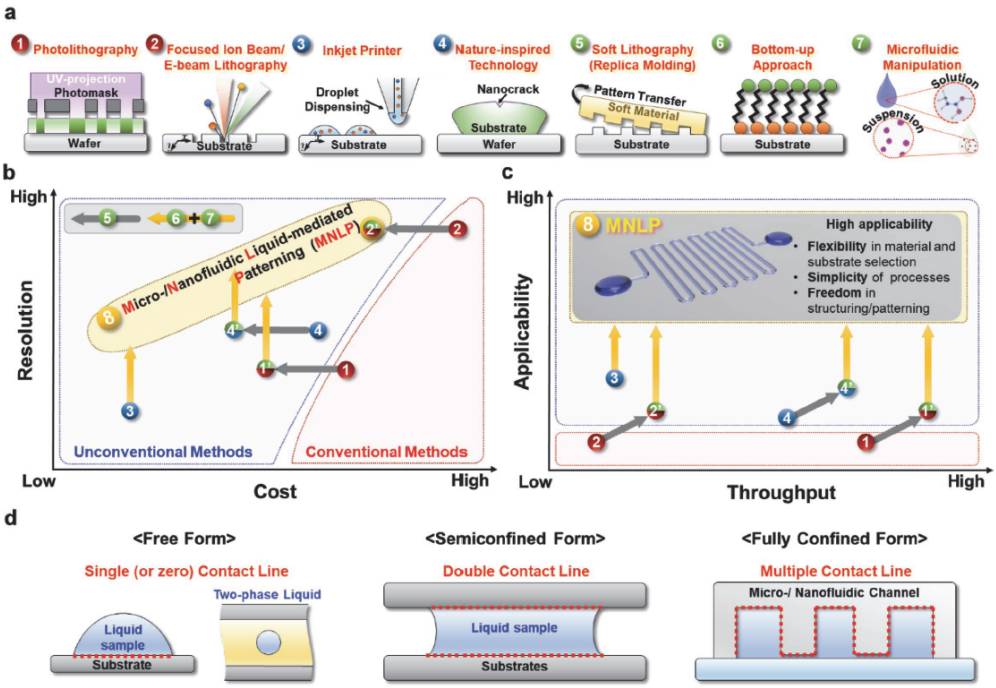

Figure 1. Characteristics according to the type of micro-/nanofluidic liquid-mediated patterning. (a) List of techniques for forming micro-/nano scale patterns. (b, c) Characteristics of micro-/nanofluidic liquid-mediated patterning. Represents resolution according to cost and applicability according to

throughput. (d) Three types according to the interface of the liquid form. Figures were adapted from Bae *et al.*[10].

1.2 A general patterning approach to control two-dimensional liquid foam in microfluidic systems

Ostwald ripening occurs frequently in gas-liquid foams on microfluidic platforms, whereby larger particles consume smaller particles around them. There have been previous studies such as the use of external fields of temperature or magnetism to manipulate the Ostwald ripening of gas-liquid foams in microfluidic systems, and the use of foam stabilizers of nanoparticles, proteins, and surfactants[11-15]. However, since these methods only attenuated the gas diffusion between the two-dimensional liquid foam, a strategy for placing micro-/nano structures on the substrate was proposed to efficiently control Ostwald ripening. By placing the posts on the substrate, the two-dimensional liquid foam was prevented from growing indefinitely, and the radius of curvature of the foam could be manipulated. It was also possible to ensure liquid patterning by causing reverse Ostwald ripening, in which liquid foams selectively evolve towards foams with a larger radius of curvature. Therefore, through the Ostwald ripening control based on the curvature of the two-dimensional liquid foam, the understanding of the 2D foam network in the microfluidic device for high-precision patterning was further improved and the assembly of functional materials was possible.

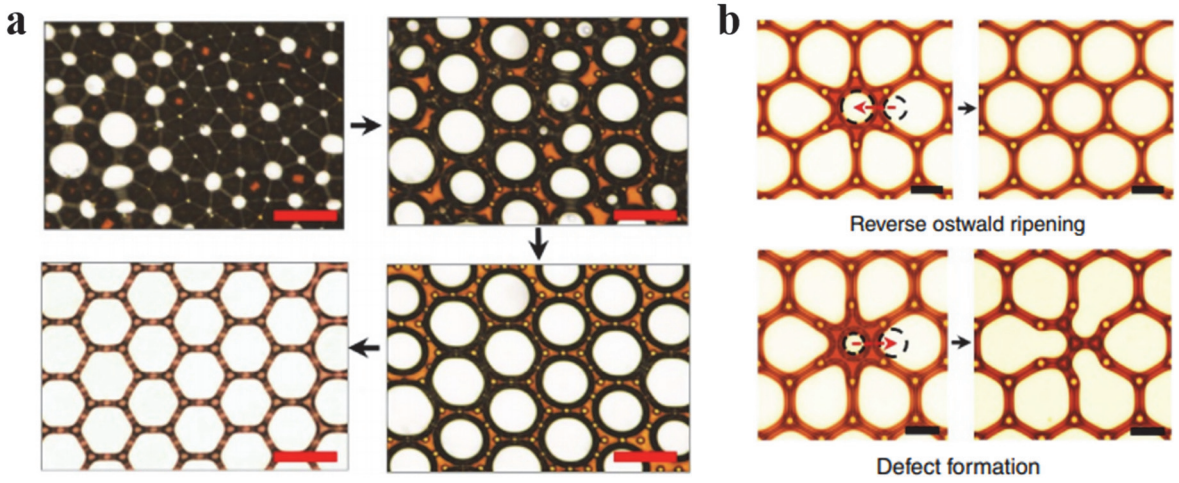

Figure 2. The working principle of patterning in a hexagonal array of 2D liquid foams using the Ostwald ripening phenomenon. (a) The process of formation of a two-dimensional liquid foam on a substrate with a post. (b) Liquid foam formed uniformly using reverse Ostwald ripening on a substrate with posts and liquid foam with defects. Figures were adapted from Huang *et al.*[3].

1.3 Water-mediated patterning using microfluidic devices

Liquid-mediated patterning is a technique that has become increasingly popular in recent years. There are research cases in which patterning can be performed based on water, or patterning based on organic materials has expanded the field of application[16-18]. In water-based patterning, liquid patterning could be done easily and simply by sweeping motion on a micropillar substrate. In addition, micro-holes and micro-posts were designed for large area patterning using properties such as surface tension and evaporation rate of water. By placing micro-holes on the substrate, the Ostwald ripening phenomenon, in which large liquid foam consumes surrounding smaller liquid foam, could be eliminated. The micro-holes convert the closed system microfluidic device into an open system to evaporate water, and the micro-posts allow liquid patterning to be performed while allowing the evaporating water to be fixed to the posts. By diluting materials such as particles, polymers, and nanowires in water to a certain concentration and then patterning them in a chip, micro-/nano scale solidified films can also be formed[19]. In this dissertation, flexible conductive films were developed by mixing silver nanowires in water.

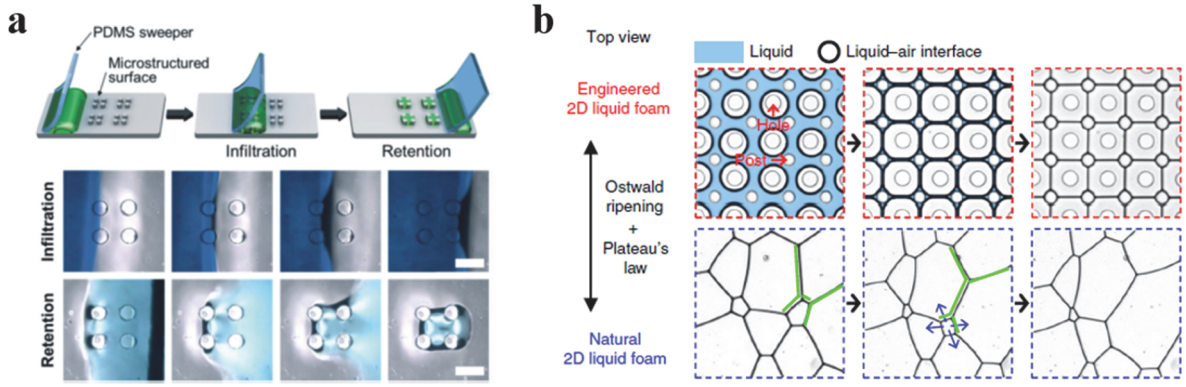

Figure 3. Patterning using water in microfluidic devices. (a) Liquid patterning on microstructured surfaces. After infiltration, droplets are confined within the microstructured area. (b) By arranging micro-holes and micro-posts, Ostwald ripening phenomenon is excluded and plateau's law is applied. Figures (a) and (b) were adapted from Park *et al.*[20] and Bae *et al.*[21], respectively.

1.4 Liquid film patterning based on O/W emulsion

Patterning has been mainly done using only water or organic materials, but some studies have conducted patterning using both water and oil at the same time[22-24]. When patterning was performed using only one material, there was a limit to the range of application. To compensate for this limitation, studies are being conducted using the new properties of emulsion, which is a mixture of two liquids.

O/W emulsion was used to fabricate porous membranes with omniphobic surfaces with liquid repellency, and O/W emulsion was also used for phase separation patterning, liquid directional transport, and block polymer patterns. Liquid films with liquid/air interfaces can be interesting research subjects in the field of droplet interfaces using interfacial materials such as liquids. Liquid films on microfluidic platforms have high aspect ratio characteristics, and if durability in the liquid state is guaranteed, there is potential for applications in the electronics industry such as flexible transparent electrodes. Therefore, we intend to develop a technology for producing a liquid film having an air/oil interface using oil, organic solvents, and heat, and experimented to determine the appropriate conditions.

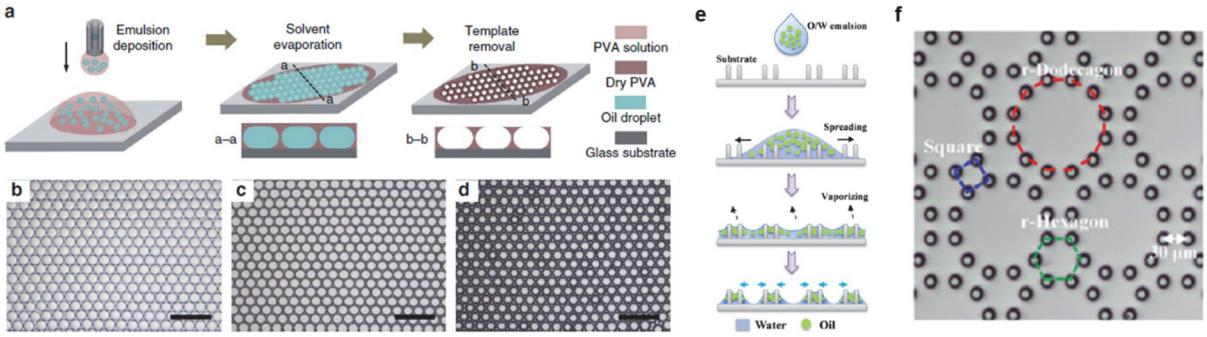

Figure 4. Two examples of patterning using O/W emersion. (a - d) When the emulsion is deposited, the solvent evaporates rapidly and self-assembly of the droplet creates a porous PVA membrane. (e, f) O/W emersion patterning on substrates with pillars. Due to the difference in the evaporation rate of the two liquids in the emulsion, the emulsion breaks, and polymer patterns are formed according to the distribution of the pillar units on the substrate. Figure (a)-(d) and (e)-(f) were adapted from Zhu *et al.*[25] and Li *et al.*[26], respectively.

1.5 Capillary-bridge printing technology using organic semiconductor materials

Previously, water-based and oil-based patterning techniques were introduced, and organic material-based patterning has great potential in electronic applications[27]. An organic semiconductor single crystal array can be fabricated by using organic materials instead of water. A 1D single-crystal array can be made using a template with a flat substrate and micropillars. After the organic solvents evaporate, an isolated liquid film is formed on the capillary bridges on the micropillars. In this way, organic 1D single crystal arrays can be fabricated by a capillary-bridge lithography method. As another example, to control the dewetting process of an organic semiconductor solution, large-scale polymer 1D arrays can be patterned using a capillary-bridge-based technique through a device having a micro-post structure[28-

[30]. It can function as micro-/nano arrays in the electronic and optical fields with facile and highly efficient patterning techniques using organic materials[31]. Here, using positive and negative photoresist, a patterning technique for solidified photoresist films, which will be used for future organic semiconductor applications, was developed.

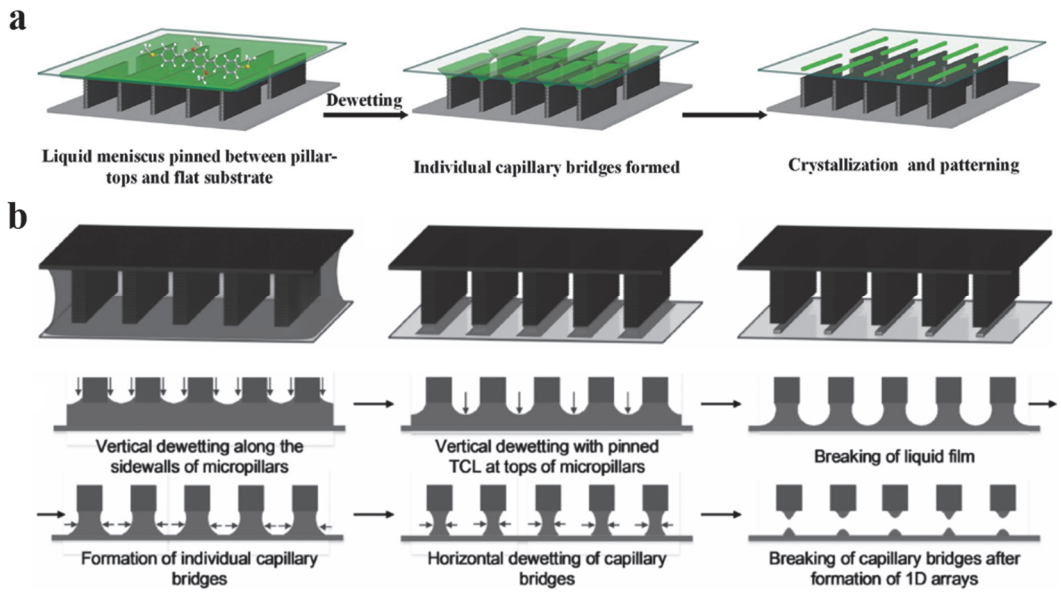

Figure 5. Patterning using a microfluidic platform and organic materials. (a) Fabrication of organic single-crystal array based on capillary-bridge lithography using organic material. (b) Schematic of capillary-bridge printing technology to make 1D polymer arrays. The liquid film emerging from the layer of polymer solution between the micro-posts and the substrate is dewetted into individual capillary bridges under the guidance of the micro-posts to form a 1D array after evaporation of the solvents. Figures were adapted from Feng *et al*.[32].

1.6 Patterning of flexible transparent conducting electrodes using template-guided foaming technology

Flexible transparent conducting electrodes (FTCEs) are essential components in a wide range of electronic research fields such as wearable devices[33], solar cells[34-36], organic light-emitting diodes (OLEDs)[37], touchscreens[38-40] and displays[41] due to their outstanding electrical characteristics and flexibility, and portability. There have been research results of applying nanowires as electrodes after patterning conductive materials on flat substrates such as capillary printing and nanodrip printing[42, 43]. In the conventional method of patterning an electrode using flat substrates, indium tin oxide (ITO) has been widely used as a transparent electrode in the commercial fields mentioned above[44]. However, the

scarcity of indium, the high cost, especially the high brittleness of the ITO electrodes, which easily crack even when exposed to moderate mechanical stress, limits their application to flexible devices[45]. In addition, since the demand for wearable devices that are lightly portable while having high durability is increasing, there have been efforts to pattern transparent electrodes on curved substrates[46, 47].

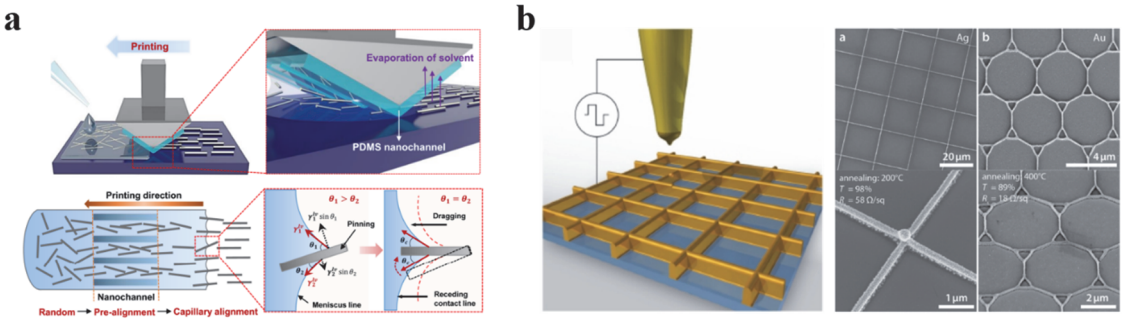

Figure 6. Nanowire patterning using a microfluidic platform. (a) Schematic of the formation of unidirectional silver nanowire arrays using nanopatterned PDMS based on the capillary alignment principle. (b) High-aspect ratio patterning scheme based on electrohydrodynamic nanodrip printing, and printed gold and silver patterning. Figure (a) and (b) were adapted from Kang *et al.*[42] and Schneider *et al.*[43], respectively.

For these reasons, including the technology of obtaining a single metal wire network by forming a crack template on transparent substrates to fabricate FTCEs[48], carbon nanotubes (CNTs)[49, 50], metal nanowires[51-53], graphene[54-56], silver nanowires (AgNWs)[57, 58], Copper nanowires (CuNWs)[59-62], and other conductive materials have been used as alternatives to ITO[63-65]. And after patterning on substrates such as glass, quartz, and polyethylene terephthalate (PET), there have been preliminary studies to demonstrate electrical and mechanical properties through bending and tensile tests[66-68]. However, due to the limitations of standard lithography processes based on two-dimensional (2D) substrates, the potential for direct patterning of curved substrates remains challenging. In particular, high-cost and time-consuming technology issues are more critical when applied to the wearable electronics industry[69].

Therefore, direct patterning on three-dimensional (3D) substrates is simple and exhibits a high throughput of the electrode patterns, and can address the weaknesses of the technology that requires large equipment. As a promising candidate, our group has developed a technology called “template guided foaming” (TGF) based on the liquid-mediated patterning (LP) approach that allows for mixed scale micro-/nano 3D conformal printing with facile and simple steps. In addition, in TGF technology, the monolithic design of the mold including through-hole and post arrays is not only flexible but also has high mechanical strength due to the OSTEMER having Young's modulus value of 1000 MPa[70, 71].

And due to the chemical resistance of OSTEMER, there are no restrictions on the use of aqueous materials such as perovskite, photoresist, and organic semiconductors[72-74]. In a previous study, silver nanoparticle grids were directly patterned on substrates having various Gaussian curvatures using TGF technology, and sheet resistance changes according to curvature were measured[75]. However, to apply this technology to a wearable device, it must be proved that the sheet resistance value must be constant even when patterning on substrates having a certain curvature, and conductivity is recovered even when repeated bending is applied[76]. Since studies related to the reduction of the sheet resistance difference of the metallic grids network according to the curvature of the substrates and the degree of fatigue of the generated grids are insufficient, there is a need for another improved method.

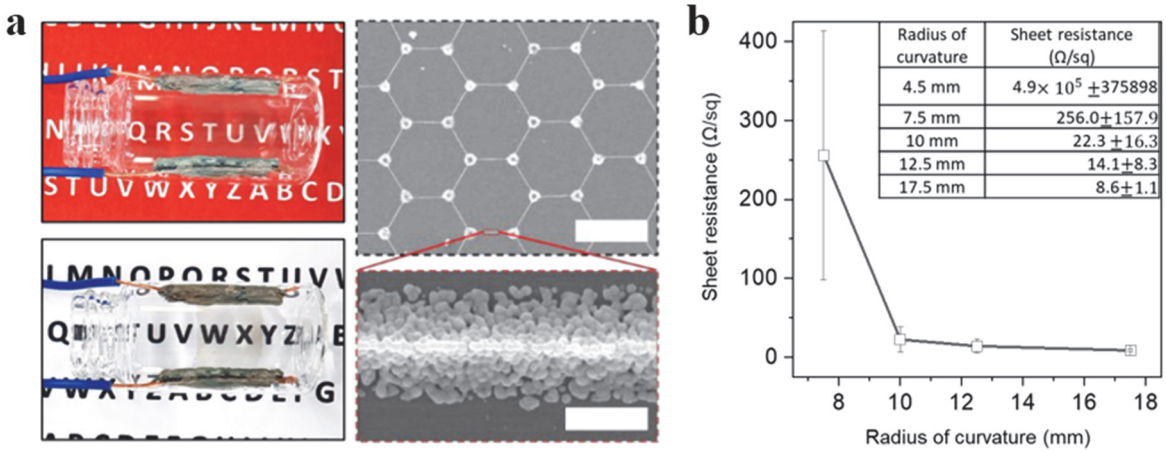

Figure 7. Silver nanoparticle grids patterned on curved substrates using TGF technology. (a) Actual images of patterned silver nanoparticle grids on glass vials, and scanning electron microscope (SEM) images. (b) Change in sheet resistance according to the radius of curvature of the patterned substrate. When the radius of curvature was less than 10 mm, the sheet resistance increased rapidly. Figures were adapted from Bae *et al.*[75].

In this work, we adopted the TGF technology to demonstrate the function of FTCEs with constant sheet resistance values regardless of the curvature of patterned substrates and high durability against repeated bending. First, to form conductive grids, microfluidic devices with through-holes that induce evaporation of the liquid, and posts in which the evaporating liquid is fixed to form regular films were fabricated. Then, we patterned the electrodes in the form of grids on curved substrates using AgNWs dispersion, and characterized the electrical properties according to the curvature and bending degree of the substrates. Also, electrodes were patterned on curved substrates using PEDOT:PSS, which is a conductive polymer, and electrical properties according to the curvature or degree of bending of the substrates were characterized in the same manner as the AgNWs electrodes. The advantage of LP is

that a variety of solutions can be used. Until now, FTCEs were produced using a dispersion containing water, and a method that could function as electrodes by forming liquid films using oil instead of water was also studied. To overcome the limitation of patterning electrodes using only the water-containing dispersion, liquid films were formed using oil instead of water[77], thereby presenting the potential to expand the range of next-generation electronic applications.

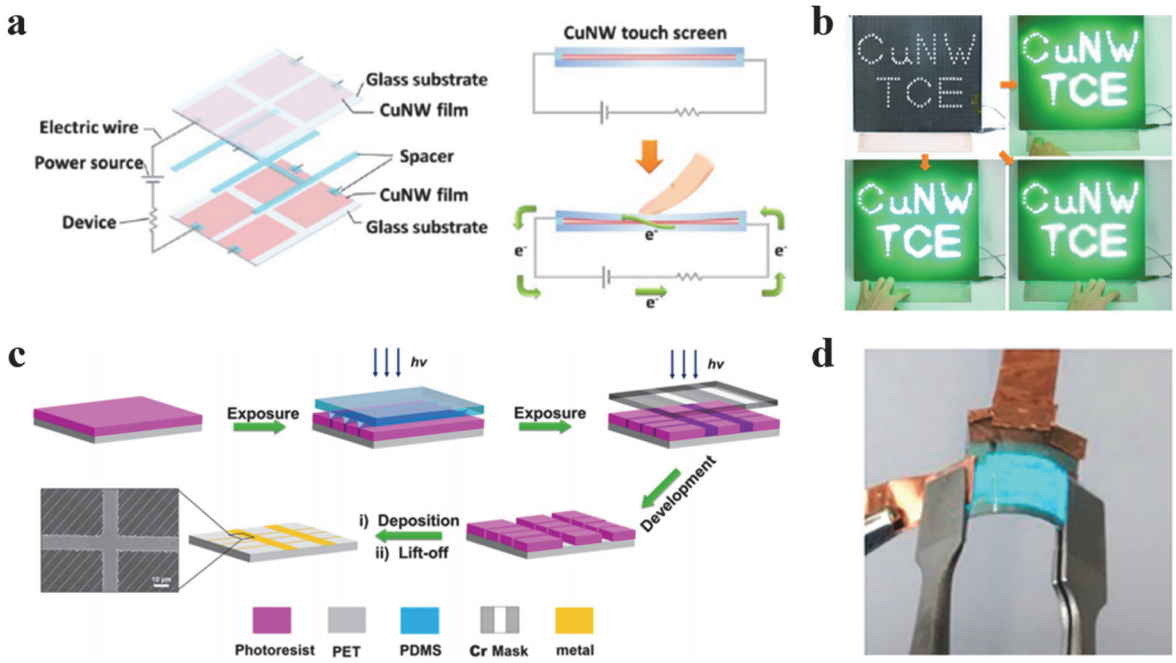

Figure 8. Materials, technologies, and applications to replace ITO electrodes with weak flexibility. (a) Schematic and working principle of CuNWs touch screen fabricated by spray deposition of copper nanowires. (b) CuNWs touch screen applied as an LED array. (c) Structural alignment of hierarchical metal grid patterns on PET substrates by using near-field photolithography with transparent PDMS as photomasks. (d) Hierarchical metal grid electrodes that retain LED light even under external stress such as bending. Figures (a, b) and (c, d) were adapted from Chu *et al.*[39] and Li *et al.*[41], respectively.

Chapter 2. Fabrication of through-hole and post arrays using microfluidic technology

2.1 Reagents and materials

Polydimethylsiloxane (PDMS; Sylgard 184, Dow Corning), off-stoichiometry thiol-ene polymer resin (OSTEMER 322 Crystal Clear, Mercene Labs), Poly(vinyl alcohol) (PVA; M_w 89,000-98,000, 99+% hydrolyzed, 341584, Sigma Aldrich) were used to fabricate the through-hole and post arrays. Chlorotrimethylsilane (TMSCI; 386529, Sigma-Aldrich), Trichloro(1H,1H,2H,2H-perfluorooctyl)silane (PFOCTS; 448931, Sigma-Aldrich) were used for surface modification of through-hole and post arrays. Silver Nanowires Dispersions (20 nm x 20 μm, Novarials) and Poly(3,4-ethylenedioxythiophene)-poly(styrenesulfonate) (PEDOT:PSS; Sigma Aldrich) were used as provided by the manufacturer. Sodium dodecyl sulfate (SDS; ACS reagent, ≥ 99.0%, Sigma-Aldrich) and was used as a surfactant at a concentration of 0.05%. Hexadecane (anhydrous, ≥ 99%, 296317, Sigma-Aldrich), Hexane (anhydrous, 95%, 296090, Sigma-Aldrich), Octane (anhydrous, ≥ 99%, 296988, Sigma-Aldrich), Toluene (anhydrous, 99.8%, 244511, Sigma-Aldrich) were used to fabricate liquid films in through-hole and post arrays. CdSe/ZnS Quantum Dots (powder, hydrophobic, 630 ± 5 nm λ, PlasmaChem) were added to non-polar organic solvents to investigate the structure of liquid films.

2.2 Fabrication of molds with through-hole and post arrays

We adopted the previously reported method to fabricate mold with through-hole and post arrays[78]. A SU-8 master mold was required to fabricate microfluidic devices, and a standard photolithography process was used (Figure 9). A negative photoresist (SU-8 2050, Kayaku Advanced Materials) was spin-coated onto a silicon wafer to a height of 50 μm and then soft baked. After exposure to UV light using a photomask and mask aligner (MA6, SussMicroTec), a post-exposure bake process is performed. Before applying the photoresist for the second layer, HMDS (HMDS; 440191, Sigma-Aldrich) was spin-coated to increase the adhesion between the wafer and the photoresist and then soft-baked. The second layer was spin-coated to a height of 25 μm using a photoresist (SU-8 2025, Kayaku Advanced Materials) and soft baked. After UV light exposure using a second photomask and mask aligner, a post-exposure bake was performed, and after that, it was immersed in SU-8 developer (Kayaku Advanced Materials) to remove the unexposed photoresist. After the hard-baked of this wafer, the photolithography process was completed. To obtain a PDMS mold, PFOCTS was used to chemically

functionalize the SU-8 master mold surface into a hydrophobic surface. For the soft lithography process, the 10:1 mixing ratio solution of the PDMS base and curing agent was degassed in a vacuum for 30 minutes. The PDMS mixture was poured into the SU-8 master mold and then cured in a 65 ℃ oven for 3 hours. The replicated PDMS mold was detached from the SU-8 mater mold, and the surface was chemically functionalized using TMSCI. To fabricate the OSTEMER membrane with through-hole and post arrays, the replicated PDMS mold was detached from the SU-8 master mold and chemically functionalized with a hydrophobic surface using TMSCI. A water-soluble sacrificial layer was created by spin coating with PVA on the glass, and a PDMS mold was placed on it. Then, to generate negative pressure in the microchannel between the PDMS mold and the water-soluble sacrificial PVA layer on the glass, the air in the PDMS mold was degassed by placing it in a vacuum state, and OSTEMER resin was injected through the inlet hole. By van der Waals interaction, the PDMS mold and the water-soluble sacrificial PVA layer on the glass remained in contact while the OSTEMER resin was loaded. After loading was completed, the OSTEMER resin was solidified by placing it in UV light of 365 nm wavelength for 5 minutes. The PDMS mold was detached, and it was reusable. The solidification of the OSTEMER resin was completed by placing it in a 90 ℃ oven for 3 hours. The sacrificial PVA layer was dissolved in deionized water to detach the through-hole and post arrays membrane from the glass.

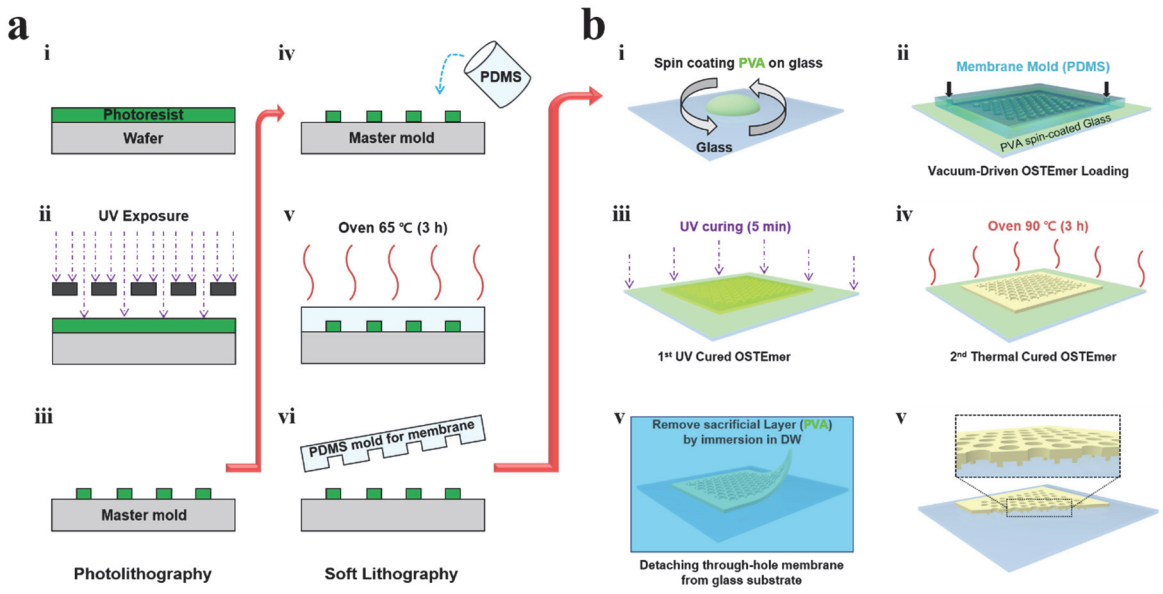

Figure 9. Fabrication process of the microfluidic platform for through-hole and post arrays. (a) Schematic of photolithography for fabricating SU-8 master mold and soft lithography process for fabricating PDMS mold. (b) Schematic of fabrication of OSTEMER membrane with through-hole and post arrays from PDMS mold.

2.3 Experimental setup

An inverted fluorescence microscope (IX71, Olympus Corp.) equipped with a charge-coupled device camera (Clara Interline CCD, Andor Technology Ltd.) was used to observe and analyze the liquid patterning process. The microscope was automated using a motorized stage (BioPrecision2), motorized focus controller (99A400), and controller system (MAC 6000) manufactured by Ludl Electronic Products. To control atmospheric conditions, a customized humidity/temperature controlling system, comprising solenoid valves (S10MM-20-24-2, Pneumadyne Inc.), a humidity/temperature sensor (SHT15, Sensirion), and a microcontroller board (Arduino Uno R3, Arduino cc.) were programmed using LabVIEW software (National Instruments Corp.). During experiments using this microscope, images were captured using imaging software (MetaMorph v7.8.10.0, Molecular Devices). The fluorescence intensities of the images were quantitatively analyzed using Image J (National Institutes of Health, Bethesda). The normalized fluorescence intensities were shown as graphs using OriginPro 2020 software (OriginLab Corp.). High-resolution SEM images were taken by a field emission scanning electron microscope (FE-SEM; S-4800, Hitachi) by sputtering a 2 nm platinum layer on the surface of the through-hole and post arrays. UV–Vis-NIR spectrophotometer (Cary 5000, Agilent) was used to measure the transmittance of the AgNWs grids and PEPOT:PSS grids. A confocal microscope (LSM 780 NLO, Carl Zeiss) was used to observe the shape of liquid films in the membrane. Images from this microscope were captured and analyzed in ZEN software (Carl Zeiss).

Chapter 3. Structural optimization of patterning AgNWs grids

3.1 Working principle of patterning AgNWs grids

The height of the through-hole and the post of the device is 50 μm and 25 μm, the diameter is 60 μm and 30 μm, respectively, and the spacing between the posts is 40 μm. Figure 11 illustrates the process of patterning AgNWs grids onto the substrates, including the following simple steps: (i) pipetting an AgNWs dispersion drop onto the substrate and laying the OSTEMER membrane on it so that the drop can spontaneously spread; (ii) patterning aligned AgNWs grids in a single step; (iii) removing the OSTEMER membrane. In step (i), The AgNWs dispersion spontaneously spreads into all spaces under the membrane with through-hole and post arrays. 20 mg/mL of 20 nm x 20 μm AgNWs dispersion was pipetted onto the substrates and the membrane was placed on it. Surfactants were added to the solution to balance Laplace pressure and disjoining pressure so that the liquid films were maintained at the nanoscale without rupturing. Then, the AgNWs dispersion spreads simultaneously throughout the membrane and causes capillary alignment.

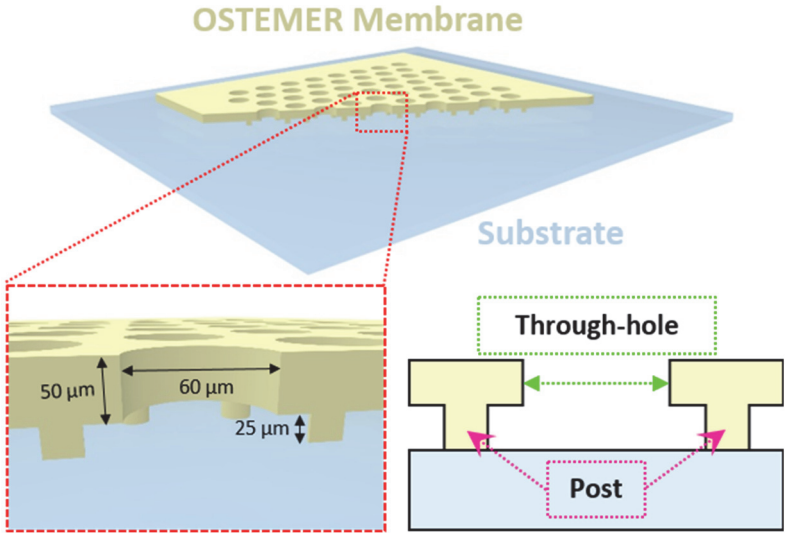

Figure 10. Schematic of the structure of through-hole and post arrays. Through-hole and post arrays structure attached to a substrate in a three-dimensional view. The posts are in contact with the glass, and holes lead to evaporation of the loaded liquid.

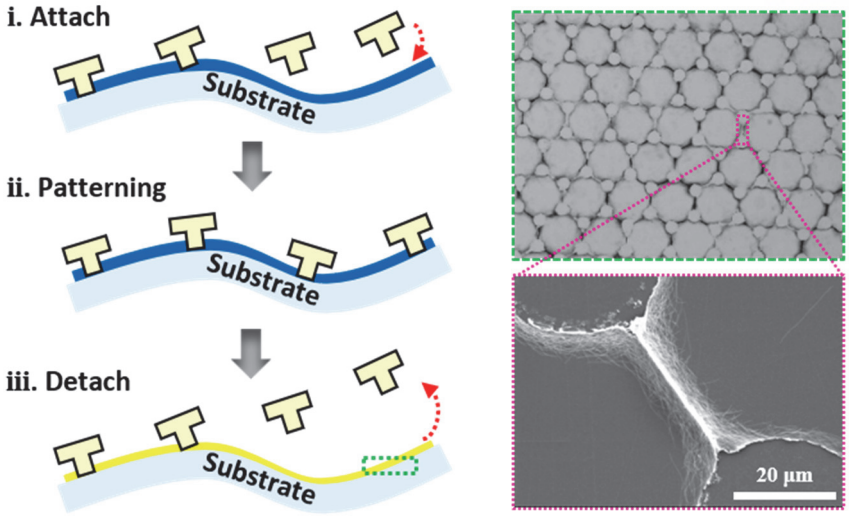

Figure 11. Schematic of the process of directly patterning AgNWs onto substrates. The process and results of patterning conductive grids on substrates. The scanning electron microscope (SEM) image shows the resultant AgNWs grids after sintering the 20 nm x 20 μm silver nanowires assembled in step iii. The scale bar is 20 μm.

In step (ii), the evaporation of AgNWs is completed in about 3 minutes by numerous through-holes, and AgNWs grids ordered by posts are patterned (figure 12, right). Even if the basic unit of the membrane consisting of through-hole and post arrays is scaled up in a large area, the evaporation flux per unit is the same, so the evaporation is completed within 3 minutes by the same patterning method. As a result, AgNWs are assembled in a nanoscale liquid foam structure, forming AgNWs patterns. The difference from the line-structured grids in which AgNPs were assembled in previous work is that AgNWs are assembled into mesh-structured grids due to the much longer and thinner wire types. In step (iii), when evaporation is complete, the membrane is removed. Silver-mesh flexible transparent conducting electrodes (SMFTCEs) are easily bent, and AgNWs grids are patterned on a 0.8 cm x 0.8 cm scale (Figure 12, left). Even if the membrane was bent to curved substrates, the internal structures were not damaged, and it was repeatedly fabricated in a facile and low-cost method.

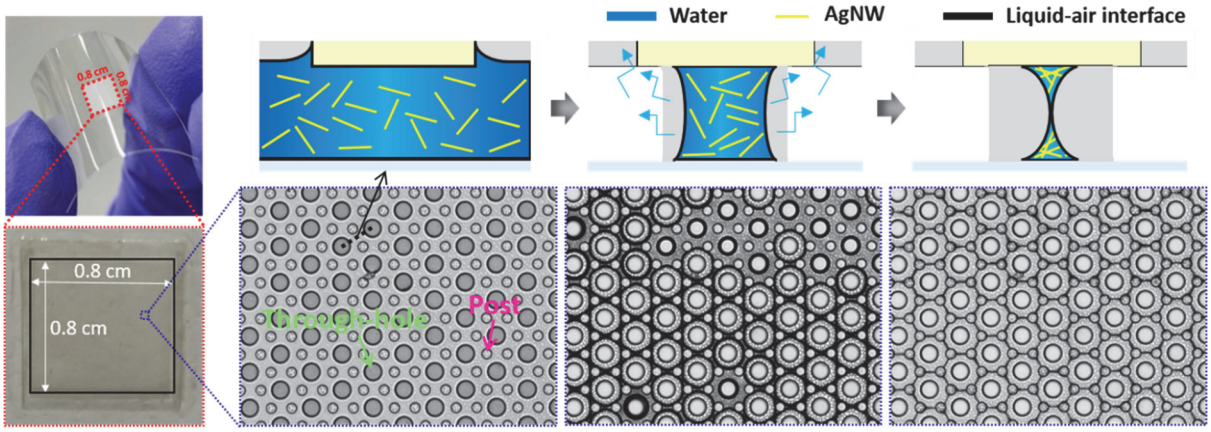

Figure 12. Real images of AgNWs patterned devices. Demonstration of step ii in Figure 8. The schematics depict a cross-sectional side view through a dotted line in optical images. Optical images show the process of patterning AgNWs grids as the aqueous solution evaporates after injection of AgNWs dispersion.

3.2 Structural optimization of patterning AgNWs grids

We investigated the optimal conditions under which AgNWs grids are patterned. Initially, we observed the resultant structures of AgNWs grids based on possible patterning conditions (Figure 13). Figure 13 shows the geometrical changes of patterned grids based on the type of substrates used. We patterned 20 mg/mL AgNWs dispersion on polycarbonate (PC), polyethylene terephthalate (PET), and glass, among those commonly used as materials for transparent conducting electrodes in recent years. We used two types of PET and glass with different contact angles. Approximately, when the contact angle was in the hydrophobic region, the AgNWs gathered between the posts, stably generating grid networks. When polycarbonate with a high contact angle was used as the substrate, the AgNWs grids were uniformly and densely agglomerated. When PET with a high contact angle was used, the grids were relatively less agglomerated to the center, and when using PET with a low contact angle, the grids were formed evenly, but the density was low. Then, when glass was used, the grids were not well agglomerated and scattered regardless of the contact angle. AgNWs grids patterned on polycarbonate are thin and flexible, suitable for bending, and have also proven their function as optoelectronic devices with the results of transmittance versus dispersion concentration.

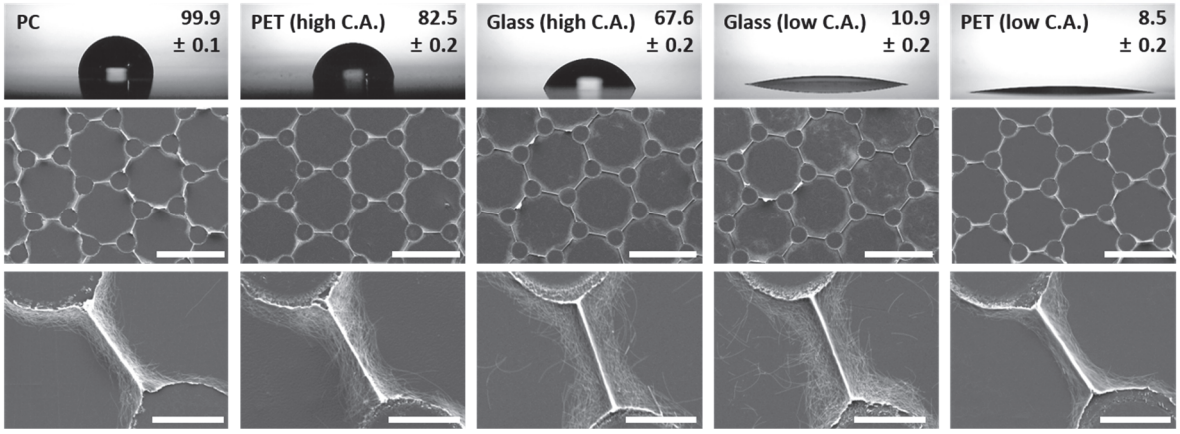

Figure 13. Characterization of the formation of AgNWs grids. Structures of AgNWs grids according to the type of substrates. Droplet images according to the contact angle values of the substrates, and SEM images of AgNWs grids patterned accordingly. The scale bars are 100 μm (middle) and 20 μm (bottom).

And then, we were able to change the width of the grids by adjusting the AgNWs dispersion concentration (Figure 14a and 14b). SEM images were taken after patterning with different concentrations of AgNWs dispersion on polycarbonate. Then, the widths of each AgNWs grid at 5 different locations were measured, and the average value and standard deviation of the widths of the grids were calculated (i.e., N = 15). When the concentration varied from 5 mg/mL to 40 mg/mL, the width of the grids ranged from 1 μm to 8 μm. Due to efforts to reduce the width of the patterned AgNWs grids, the concentration was reduced to 5 mg/mL, but rather, there were quite a lot of AgNWs grids that were lost, and the resulting sheet resistance value also increased significantly. In addition, we observed conditions in which AgNWs grids were not scattered while keeping other geometrical parameters constant and varying the distance between posts (Figure 14c). When the distance between posts was reduced to 40 μm, mesh-like densely aggregated AgNWs grids were formed at the sub-micron resolution.

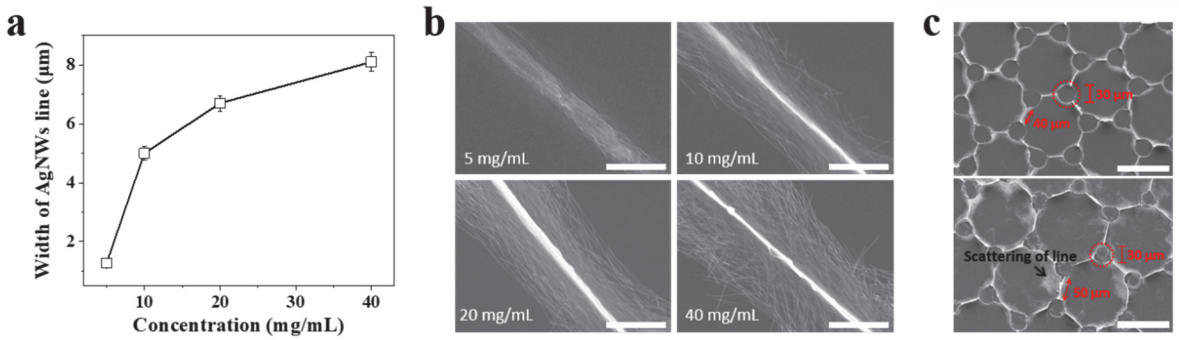

Figure 14. (a, b) Images of width change of AgNWs grids according to the concentration of AgNWs dispersion (N = 15 from 5 different locations of 3 different grids for the average value with standard deviation). Scale bars are 5 μm. (c) Improved patterning images of AgNWs gird by adjusting the distance between posts. The diameters of posts are both 30 μm, and the distances between the top and bottom images are 40 μm and 50 μm, respectively. Scale bars are 100 μm.

3.3 Conductivity change with curvature and electrical resistance to external pressure of patterned AgNWs grids

We investigated the electrical properties according to the degree of bending of AgNWs grids patterned on substrates with various curvatures (Figure 15). Figure 15a shows the sheet resistance of SMFTCEs patterned on polycarbonate according to the concentration of AgNWs dispersion. Patterned AgNWs grids improved conductivity by annealing at 160 °C for 2 hours to remove insulating surfactants around AgNWs. At concentrations lower than 10 mg/mL, the density and cohesion of the mesh-structured AgNWs grids decreased, resulting in a significant increase in sheet resistance. To investigate the electrical properties of curved AgNWs grids, we patterned 20 mg/mL of AgNWs dispersion on 4 different curvature substrates (Figure 15b). The sheet resistance values after patterning on substrates having a curvature ranging from 0 to 0.14 mm^{-1} ranged from 27.47 to 29.95 Ω/sq, and there was no difference in conductivity of AgNWs grids according to the curvature.

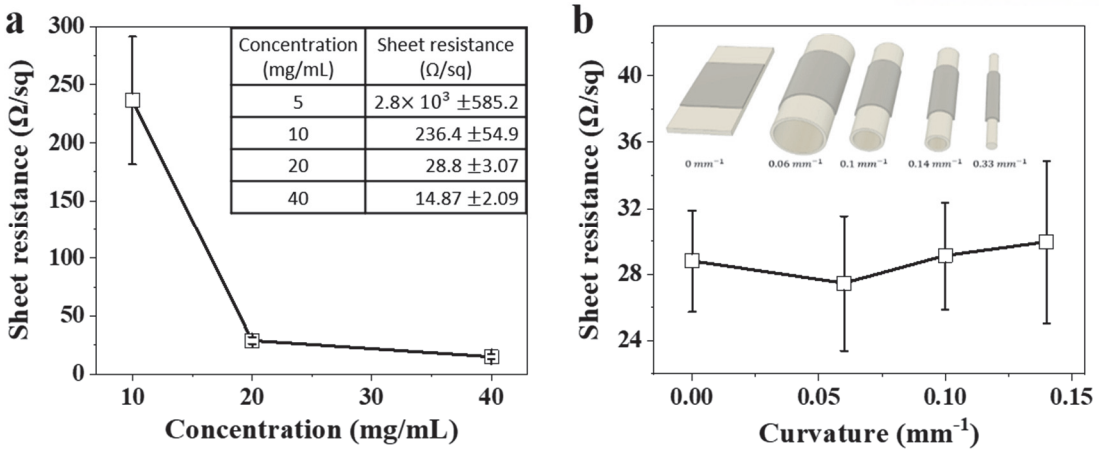

Figure 15. Characterization of sheet resistance measurements and bending tests of patterned AgNWs grids. (a) The sheet resistance according to the concentration of AgNWs dispersion. (b) Sheet resistance of AgNWs grids patterned on substrates with various curvatures.

We characterized the sheet resistance of AgNWs grids patterned on substrates with various curvatures when bent at different curvatures (Figure 16a). We first demonstrated that the conductivity changes only by curvature, regardless of the direction in which the hexagonal grid array is bent horizontally or vertically. When the AgNWs grids patterned on flat substrates were bent to a 0.33 mm^{-1} curvature, there was an increase in sheet resistance of about 12%. And when the AgNWs grids patterned at curvatures of 0.06 mm^{-1}, 0.10 mm^{-1}, and 0.14 mm^{-1} were bent to 0.33 mm^{-1}, the sheet resistance increased by about 6%. And, it is remarkable that the conductivity increases when the SMFTCEs are bent with a negative curvature in the opposite direction based on the initial curvature. The reason is that when bending with positive curvature, the grids of the mesh structure are wide open, resulting in a decrease in conductivity, and when bending with negative curvature, the grids become closer to each other, increasing the conductivity. Inferring from these results, it can be seen that fewer conduction losses occur when bending the curved AgNWs grids than in the flat state. We measured the change in conductivity through the bending test to investigate the durability of the SMFTCEs (Figure 16b). When bending was repeated 10,000 times with a bending radius of 3 mm, the change in resistance increase ranged from 3 to 4% regardless of the initial curvature of the grids. Analyzing these results, it was concluded that the durability of SMFTCEs was excellent because there was little change in conductivity even when the number of bending cycles increased. In addition, since the curvature of the initial state becomes self-recovery even with repeated bending, it can be applied as a wearable bending sensor that detects a change in sheet resistance according to the curvature. The previous results reveal that if SMFTCEs are applied as a bending sensor attached to a finger, the change in sheet resistance can

be stably checked even if the radius of curvature is low and repeatedly moves regardless of the direction of motion of the finger.

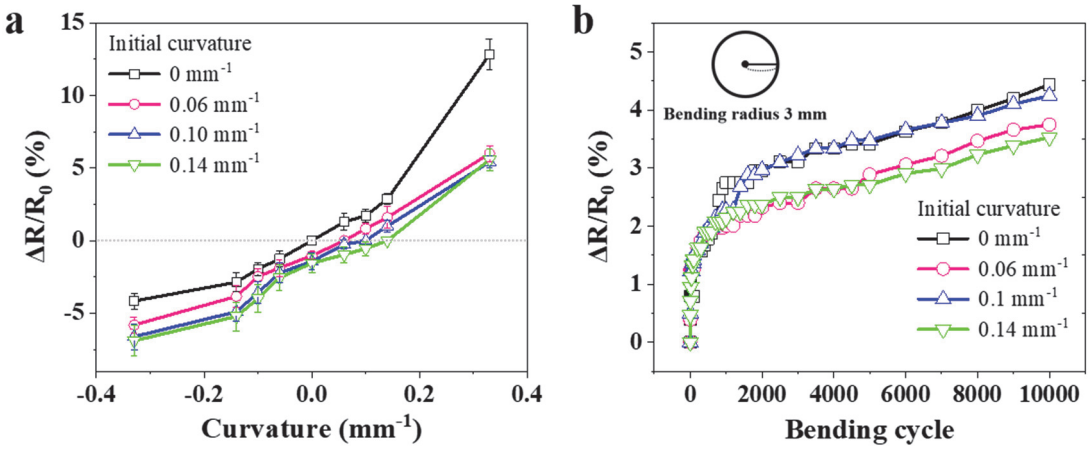

Figure 16. (a) Measurement of sheet resistance change when AgNWs grids patterned on substrates of various curvatures were bent over substrates of different curvatures. The gray dotted line represents the flat state. (b) Fatigue testing through repeated bending of patterned AgNWs grids on substrates with a bending radius of 3 mm.

Chapter 4. Patterning of FTCEs using conductive polymers

4.1 Patterning of flexible transparent conducting electrodes using conductive polymer PEDOT:PSS

Polymer flexible transparent conducting electrodes (PFTCEs) were formed by patterning with conductive polymer PEDOT:PSS, and the structure and electrical properties were characterized in the same manner as SMFTCEs (Figure 17). PEDOT:PSS grids were patterned with the TGF technology used in SMFTCEs, and SEM images were taken to investigate the structure according to the concentration of dispersion. At 5 mg/mL, uniform and thin grids were patterned. At concentrations less than 5 mg/mL, the grids became thinner, but the connection was frequently broken, while at higher concentrations, tearing occurred as the width and height of the grids increased.

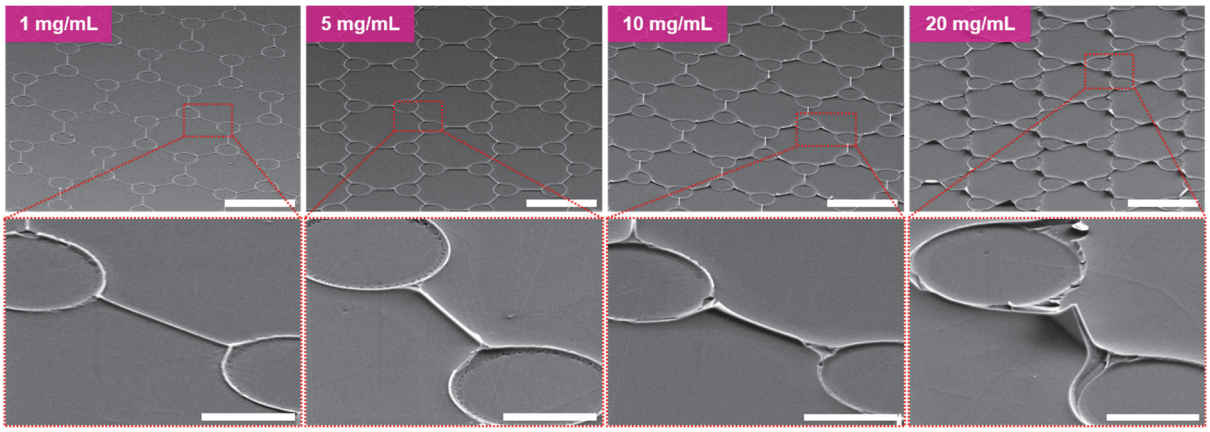

Figure 17. Characterization of the structure of conductive grids using PEDOT:PSS. SEM images of conductive grids according to the concentration of PEDOT:PSS dispersion. The scale bars are 100 μm (top) and 20 μm (bottom).

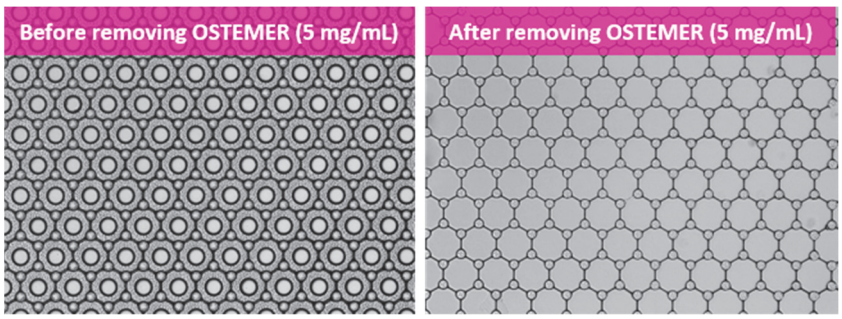

Figure 18. Polymer grids patterned using PEDOT:PSS at a concentration of 5 mg/mL (left), and polymer grids after OSTEMER was removed from the substrate (right).

4.2 Conductivity change with curvature and electrical resistance to external pressure of patterned PEDOT:PSS grids

The conductivity and resistance to external pressures of PEDOT:PSS grids were tested to demonstrate that PFTCEs also exhibited the same trends as SMFTCEs (Figure 19). At a concentration of 10 mg/mL or more, the conductivity was non-uniform because the PEDOT:PSS grids were also frequently torn off when the OSTEMER membrane was removed from the substrate. On the other hand, at a concentration of 1 mg/mL, the grids were uniformly patterned, but the conductivity was poor because they were too thin. At the concentration of 5 mg/mL, the structurally stable grids of the line structure were uniformly patterned and the conductivity was relatively stable, so subsequent experiments were conducted at this concentration. The sheet resistance of the flat PEDOT:PSS grids was 1944 Ω at 5 mg/mL, and there was no significant difference even when patterned with different curvatures.

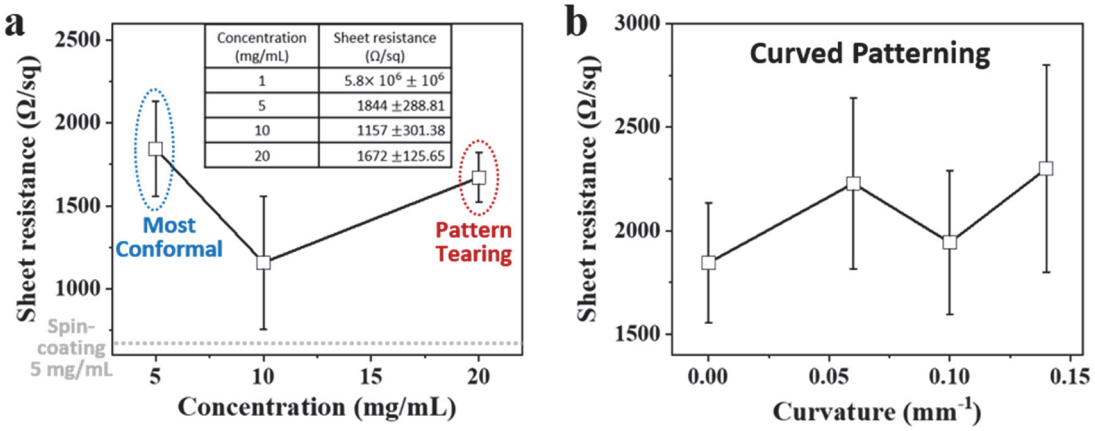

Figure 19. Characterization of the electrical properties of conductive grids using PEDOT:PSS. (a) Sheet resistance according to the concentration of PEDOT:PSS dispersion. (b) The sheet resistance of PEDOT:PSS grids patterned on substrates with various curvatures.

Notably, unlike mesh-structured AgNWs grids, line-structured PEDOT:PSS grids lost their conductivity in both cases of outer or inner bending based on the initial curvature, and the sheet resistance increased up to 10% when bent 10,000 times with a curvature of 3 mm (Figure 20). PEDOT:PSS grids were also patterned with TGF technology and were proven to be transparent and flexible, but the conductivity versus transmittance was inferior to AgNWs grids (Figure 21). This study offers a new perspective by focusing on the ability to pattern in the same way and observe a variety of patterns using TGF technology, even if the material changes.

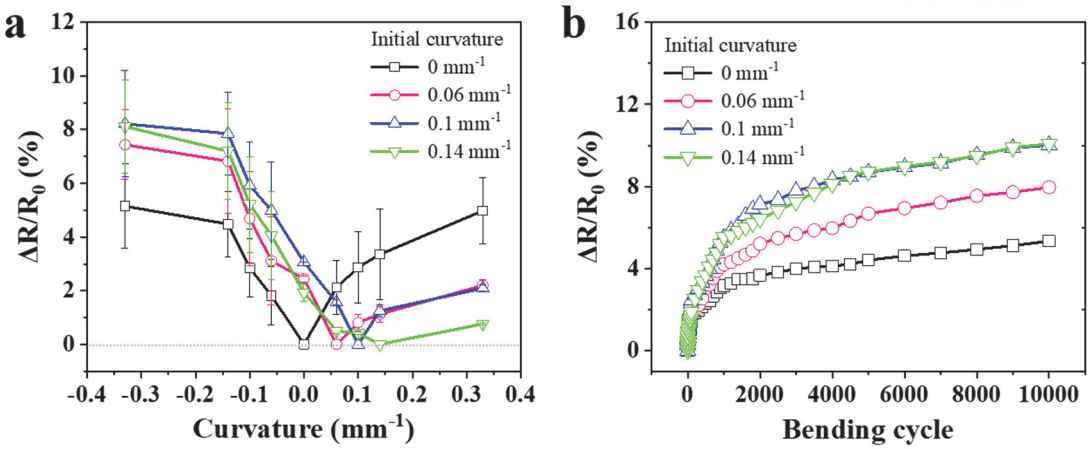

Figure 20. (a) Measurement of sheet resistance change when PEDOT:PSS grids patterned on substrates of various curvatures were bent over substrates of different curvatures. The gray dotted line represents the flat state. (b) Fatigue testing through repeated bending of patterned PEDOT:PSS grids on substrates with a bending radius of 3 mm.

4.3 Characterization of the transmittance of SMFTCEs and PFTCEs

AgNWs and PEDOT:PSS grids patterned on polycarbonate are thin and flexible, suitable for bending, and have also proven their function as optoelectronic devices with the results of transmittance versus dispersion concentration (Figure 21). Figure 21a depicts SMFTCEs and PFTCEs obtained with 5 μL AgNWs dispersion of 20 mg/mL and 5 μL PEDOT:PSS dispersion of 20mg/mL on polycarbonate substrates, respectively. We investigated the percent transmittance of SMFTCEs and PFTCEs in the visible range of 400-800 nm. As a result of measuring the transmittance of SMFTCEs, a transmittance of 80-92% was obtained at a wavelength of 550 nm while maintaining the conductivity (Figure 21b). And, PFTCEs obtained a transmittance of 77-94% at a wavelength of 550 nm while maintaining conductivity (Figure 21c). These results indicate that both SMFTCEs and PFTCEs have achieved appropriate transparency in the concentration range used and that the sub-micron grid networks are well aligned. SMFTCEs maintain conductivity and transparency at a concentration of 20-40 mg/mL of AgNWs dispersion, and PFTCEs maintain conductivity and transparency at a concentration of 5 mg/mL of PEDOT:PSS dispersion. Therefore, combining a suitable conductive material with TGF technology not only allows direct patterning of the material in a single step on various curvature substrates but also maintains its optoelectronic properties even under mechanical stresses such as bending.

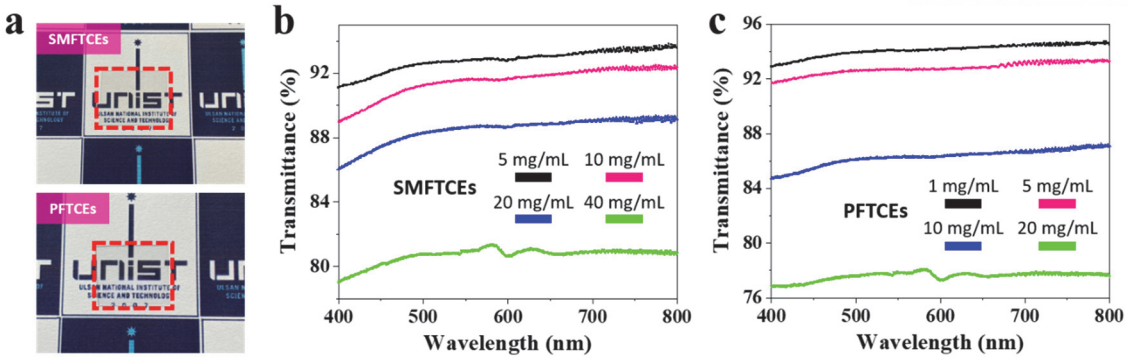

Figure 21. Comparison of transmittance of SMFTCEs and PFTCEs fabricated by the TGF technology. (a) Real images of SMFTCEs patterned with 20mg/mL AgNWs dispersion (top) and PFTCEs patterned with 5mg/mL PEDOT:PSS dispersion (bottom). (b) Optical transmittance over the visible spectrum of the SMFTCEs for various concentrated solutions. (c) Optical transmittance over the visible spectrum of the PFTCEs for various concentrated solutions. The substrate was used as a reference.

Chapter 5. Patterning liquid films for the potential of next-generation wearable systems

5.1 The structure and working principle of oil-based patterning

Liquid-mediated patterning technology has the advantage of being able to use various solutions. In addition to evaporation of water at room temperature, patterning using the boiling point of the solution is possible under various temperature conditions. As a preliminary study for the possibility of FTCEs with high electrical properties, the patterning of flexible and highly durable liquid films was characterized according to temperature conditions and the type of solvent. Figure 22 illustrates the process after injecting a mixture of oil and non-polar organic solvents into the membrane for liquid film patterning. The through-hole makes the microfluidic device an open system and naturally induces the evaporation of the liquid. As a result, Ostwald ripening phenomenon, in which large air bubbles absorb small air bubbles, was excluded[79]. Then, the evaporating liquid is fixed to the posts and the liquid films are patterned. The thickness of the liquid films can be adjusted according to the solution used.

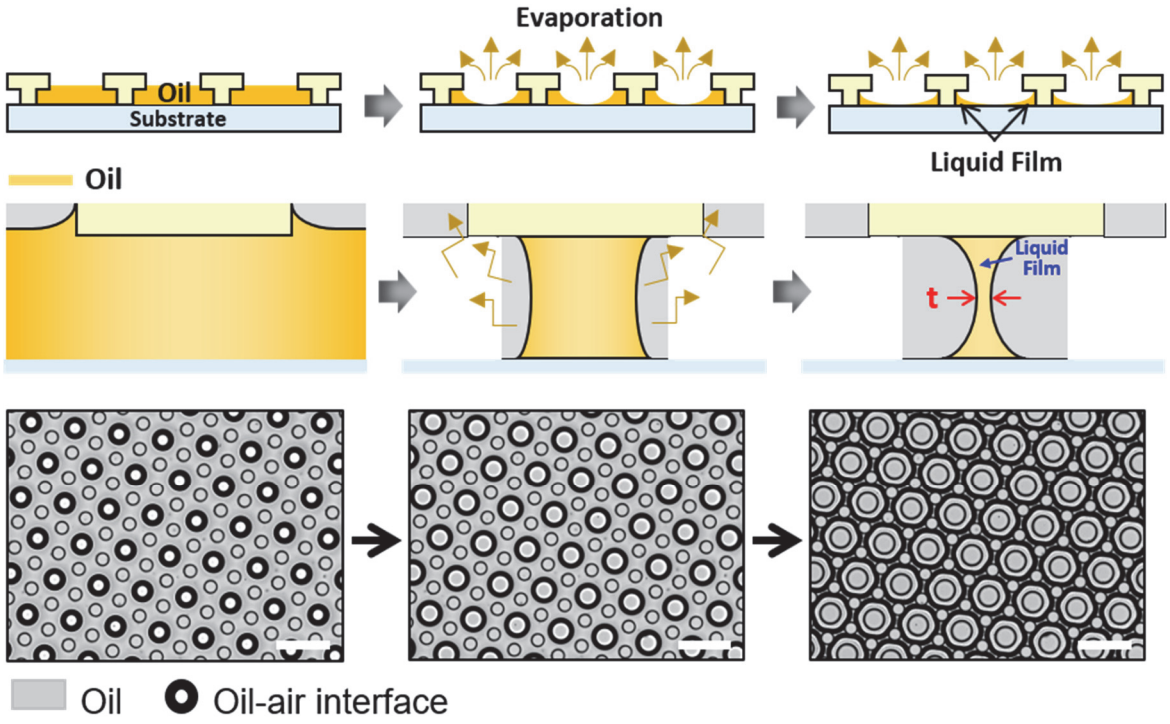

Figure 22. Schematic of the working principle and formation process of liquid films. Schematic of the formation process of liquid films and images taken under a microscope. As non-polar organic solvents

in the mixture of injected oil and solvents evaporate, the remaining oil forms liquid films. The red "t" represents the thickness of the liquid film. Scale bars are 120 μm.

To derive the mechanism for the thickness of the film formed by the liquid foam between the air-oil interface, by the following equations:

$$x_n = \sqrt[2]{\frac{4\gamma}{3\eta}\frac{1}{h \cdot f_{\text{evap}}}} \text{ or } x_n = \sqrt[3]{\frac{8\gamma}{3\eta}\sin\theta_{1,2}\frac{1}{f_{\text{evap}}}} \quad (1)$$

where x_n is the liquid film thickness, γ is the surface tension, η is the viscosity, h is the liquid film height, and f_{evap} is the evaporation rate[80]. To understand the shape of liquid films, the images were taken with a confocal microscope by injecting fluorescent quantum dots (Figure 23). After dissolving in octane at a concentration of 4 mg/mL, mixed with hexadecane at a ratio of 9:1, it was injected into the membrane. When observed with a confocal microscope, when the magnification was increased in the middle part of the liquid films, it has a concave shape inward. Two methods were used to pattern liquid films within the membrane. First, as a method using heat, hexadecane is injected into the membrane, and then the high temperature was applied to the membrane with a hot plate to induce evaporation of hexadecane to form liquid films. When the membrane was filled with hexadecane, the heat was applied to gradually induce the evaporation of hexadecane, and liquid films with oil/air interfaces were formed as the air was filled from the posts.

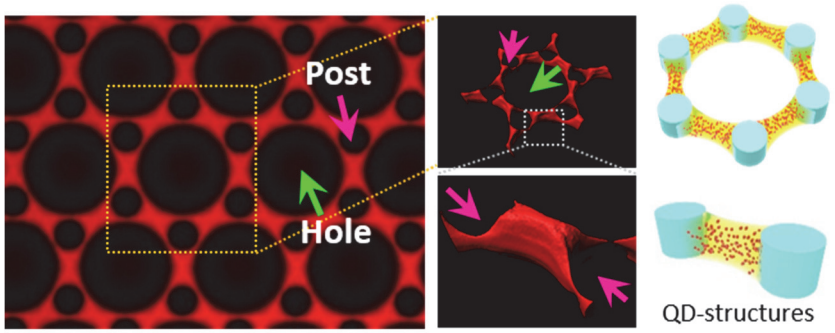

Figure 23. Images were taken with a fluorescence microscope (left), images were taken with a confocal microscope (center), and a 3D schematic (right). CdSe/ZnS Quantum Dots were dissolved in octane at a concentration of 4 mg/mL. Purple arrows and light green arrows represent posts and holes, respectively.

5.2 Patterning methods and thickness characterization of liquid films

We characterized the ability to control the thickness of liquid films by controlling the temperature and time applied to the membrane (Figure 24a and 25a). Here, the change in the thickness of the liquid films according to the applied temperature was measured while changing the temperature under the membrane to 70, 80, 100, and 130 ℃. Then, the membranes were heated at 100 °C for different times to form liquid films of 4 different thicknesses, and left at room temperature to demonstrate long-term stability (Figure 24b and 25b). 2 liquid films with a thickness of 3-4 μm were maintained until Day 8, liquid films with a thickness of 2 μm were maintained until Day 7, and liquid films with a thickness of fewer than 1 μm were maintained until Day 3. Second, as a method of using non-polar organic solvents, a mixture of hexadecane and non-polar organic solvents is made (1:6 - 1:35). Then, after injecting a mixture having a specific ratio into the membrane, the remaining hexadecane formed liquid films as the non-polar organic solvents evaporated.

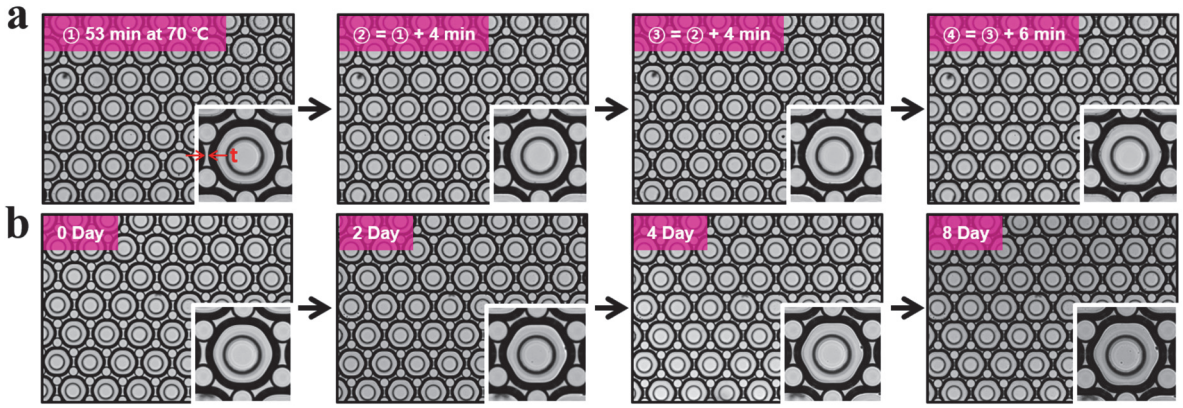

Figure 24. (a) Images showing the change in thickness of liquid films at 70 ℃. (b) Images of the thickness of liquid films formed at 100 ℃ over time (bottom).

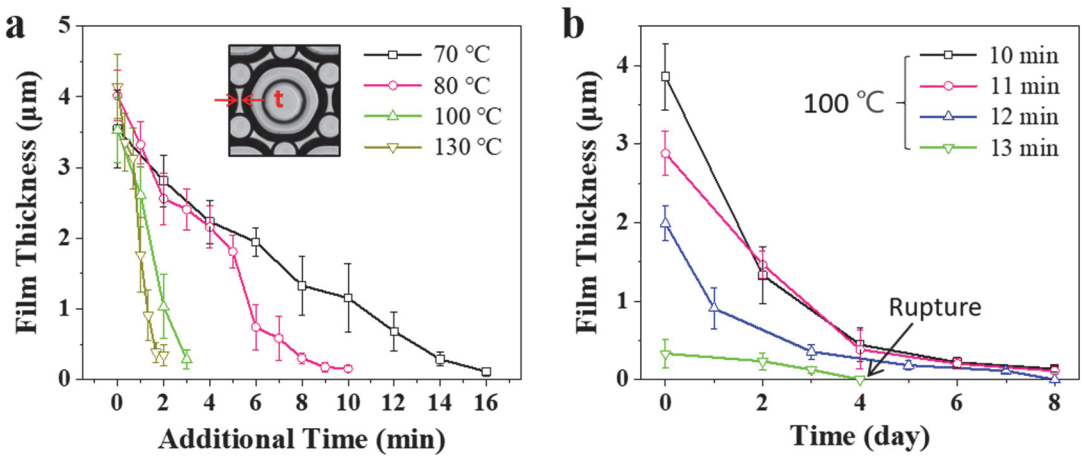

Figure 25. Characterization of the patterned thickness of liquid films using two methods. (a) Characterization of the change in thickness of liquid films when 4 temperatures (70 ℃, 80 ℃, 100 ℃, 130 ℃) were applied to the through-hole and post arrays membrane. (b) Characterization of durability when applied to 100 ℃ of liquid films of 4 different thicknesses.

We also characterized the thickness of liquid films by controlling the ratio of oil to non-polar organic solvents (Figure 26a). When the ratio of hexane was 9 times higher, it was maintained until Day 6, and when the ratio of hexane was 25 times higher, liquid films were maintained for more than Day 3 (Figure 26b). In the case of hexane, not only could liquid films be patterned by injecting a mixed solution having a ratio of various ranges, but also liquid films having various thicknesses of 1 to 4 μm could be formed. In addition, patterned liquid films secured long-term stability, and liquid films having a thickness of about 500 nm were maintained for more than Day 3. Liquid films patterned with toluene and octane were less secure than hexane (Figure 27). Therefore, if the criteria for selecting non-polar organic solvents are the degree to which the thickness of liquid films can be controlled and durability, liquid films formed using hexane are suitable for later applications. Using hexane, defects in patterned liquid films were also characterized by varying the parameters of through-hole and post in the membrane (Figure 29). The patterning of the liquid films was performed on a flat substrate, as the substrate had little effect on whether it was flat or curved (Figure 28). Oil films patterned on flat substrates were maintained even when bent to a radius of curvature of 3 mm. Liquid films have a much higher aspect ratio compared to solid grids and demonstrated high flexibility and flexural strength. Therefore, if self-assembly of conductive material is additionally performed, it can be applied as a new concept electrode with increased conductivity. In addition, we also patterned solid organic films with a high aspect ratio using photoresist and toluene. Since organic films have a higher aspect ratio than SMFTCEs and more durable than liquid films, they have sufficient potential as a part of future electrode development using conductive organic semiconductor materials (refer to Figure S6 in Supporting Information).

	Skeletal formula	Solubility in water	Boiling point
Hexane (C_6H_{14})	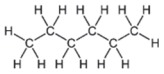	Insoluble in water	69 ℃
Octane (C_8H_{18})	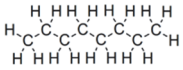	Insoluble in water	125-127 ℃
Toluene ($C_7H_8C_6H_{14}$)		Insoluble in water	110-111 ℃
Petroleum ether (C_6H_{14})	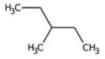	Insoluble in water	35-60 ℃
Ethyl ether ($C_6H_{10}O$)	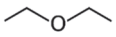	Soluble in water, 64 mg/L at 25 ℃	35-40 ℃
Pentane (C_5H_{12})	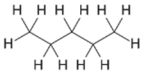	Soluble in water, 38 mg/L at 25 ℃	36 ℃

Table 1. Non-polar organic solvents used in the experiment. These organic solvents mix well with hexadecane and do not damage the post-hole arrays OSTEMER membrane.

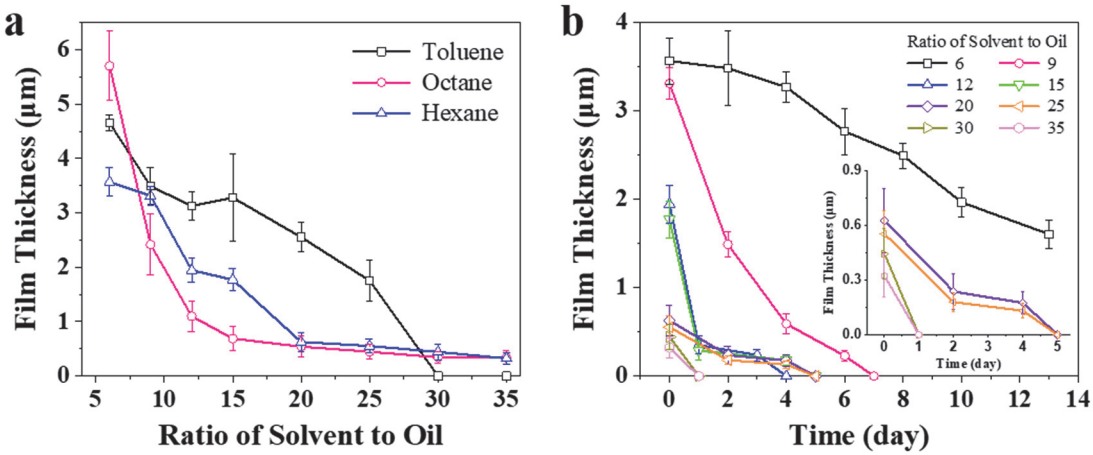

Figure 26. (a) Characterization of the thickness of liquid films with varying ratios of hexadecane to non-polar organic solvents ranging from 1:6 to 1:35. (b) The thickness and durability of liquid films when different ratios of hexadecane and hexane are injected. Error bars represent the standard deviation of the thickness of the 20 patterned liquid films.

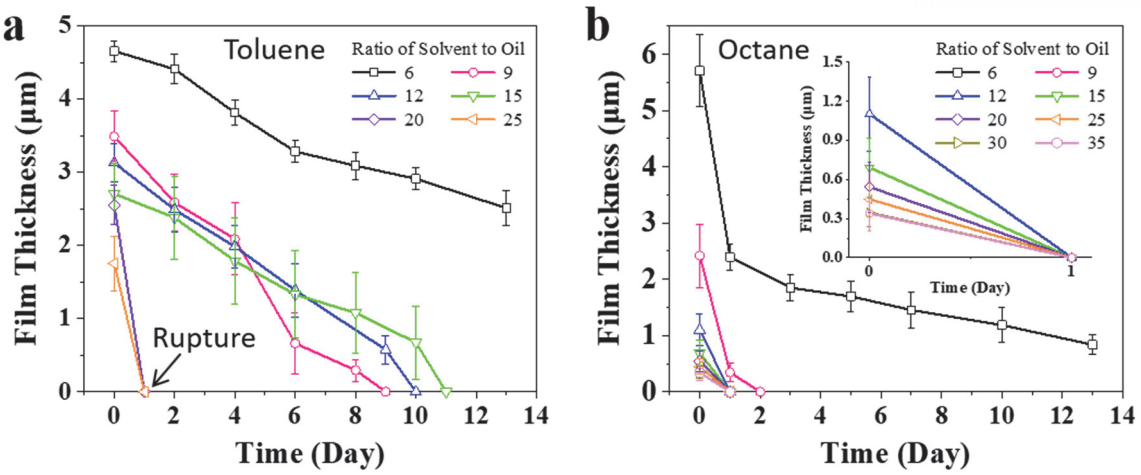

Figure 27. Characterization of the durability of patterned liquid films using non-polar organic solvents. (a) The thickness and durability of liquid films when different ratios of hexadecane and toluene are injected. (b) The thickness and durability of liquid films when different ratios of hexadecane and octane are injected. Error bars represent the standard deviation of the thickness of the 20 patterned liquid films.

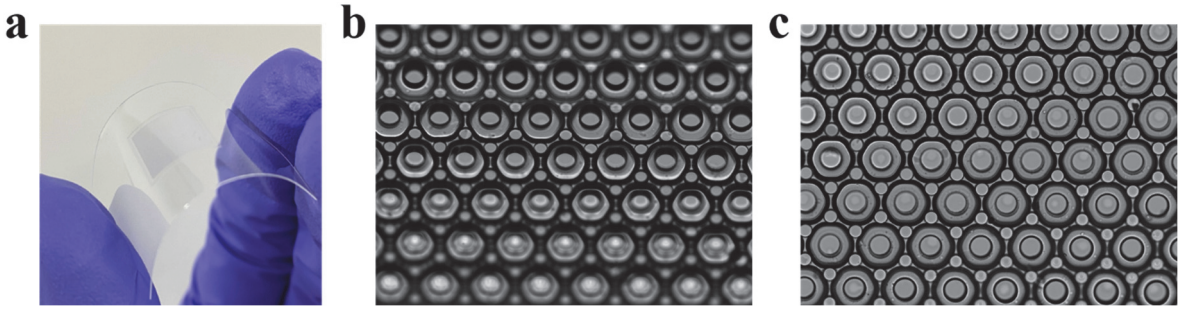

Figure 28. Oil films patterning on curved substrates and bending tests to demonstrate flexural strength. (a) Real image of a device patterned with oil films on a curved substrate. (b) An image of curved oil films patterned on a substrate with a curvature of 0.14 mm^{-1}. (c) An image of patterned oil films on a flat substrate after repeated bending 100 times with a radius of curvature of 3 mm.

5.3 Patterning of liquid films in various arrays of microfluidic devices

The through-hole and post arrays used as the main in the experiments so far are hexagonal in which one hole and six posts form an array, with a height of 25 μm, a post diameter of 15 μm, and a hole diameter of 30 μm. This structure has been used for the characterization of major experiments so far as it has stable parameters for liquid film formation upon solution injection. In figure 29, characterization of through-hole and post arrays with different shapes and different parameters was also attempted. Until

now, hexagonal arrays have been used, but liquid films can be formed even in a rectangular array consisting of 1 hole and 4 posts. The main parameters that makeup through-hole and post arrays that influence the formation of liquid films are the shape of the arrays, the height of the post (h_p), the diameter of the post (d_p), and the distance between posts (l). Here, in the process of forming liquid films, the foam that the air trapped in the hole pushes the liquid outward was designated as an air cell. Figure 29a shows the degree of liquid film formation defects when the solution is injected into a device with various parameters in square arrays. d_p was set in the range of 50 to 80 μm, l was set in the range of 40 to 60 μm, and the height of the post was fixed at 25 μm. When a device with l of 40 μm was used, when the solution was injected into the device with parameters for all the set posts, the defects in the formation of liquid films were nearly 0%. And when a device with l of 50 μm was used, the defects were about 5% when d_p was set to 80 μm, but when d_p was set to 70 μm, the defects were about 30%. And when d_p was set to 60 μm and 50 μm, the defects were nearly 100%. In the device with l set to 60 μm, when the solution was injected into the device with all the set post parameters, the defects in the formation of liquid films were nearly 100%. Analyzing this graph shows that in rectangular arrays, the closer the distance between posts, the lower the number of defects, and the smaller the post diameter, the higher the number of defects. In a device with rectangular arrays, the number of liquid films that a post must support is 4. However, in hexagonal arrays, 1 post only needs to support 3 liquid films, so structures with hexagonal arrays can form liquid films more stably. Figure 29b shows the degree of liquid film formation defects when the solution is injected into a device of hexagonal arrays with various parameters. d_p was set in the range of 20-50 μm, l was set in the range of 30-50 μm, and the height of the post was fixed at 25 μm. When using a device with l of 30 μm, the defects were 0% when d_p was set to 30-40 μm, but when d_p was set to 20 μm, the defects were about 60%. Using a device with l of 40 μm, defects were 0% when d_p was set to 30-40 μm. However, when d_p was set to 20 μm, the defects were almost 100 %. And when a device with l of 50 μm was used, 10% defects resulted when d_p was set to 50 μm, and about 20% defects were obtained when d_p was set to 40 μm. And when the device with d_p set to 30 μm was used, more than 90% of defects resulted. What can be inferred from this result is that in hexagonal arrays, the closer the distance between posts, the lower the number of defects, and the smaller the post diameter, the higher the number of defects.

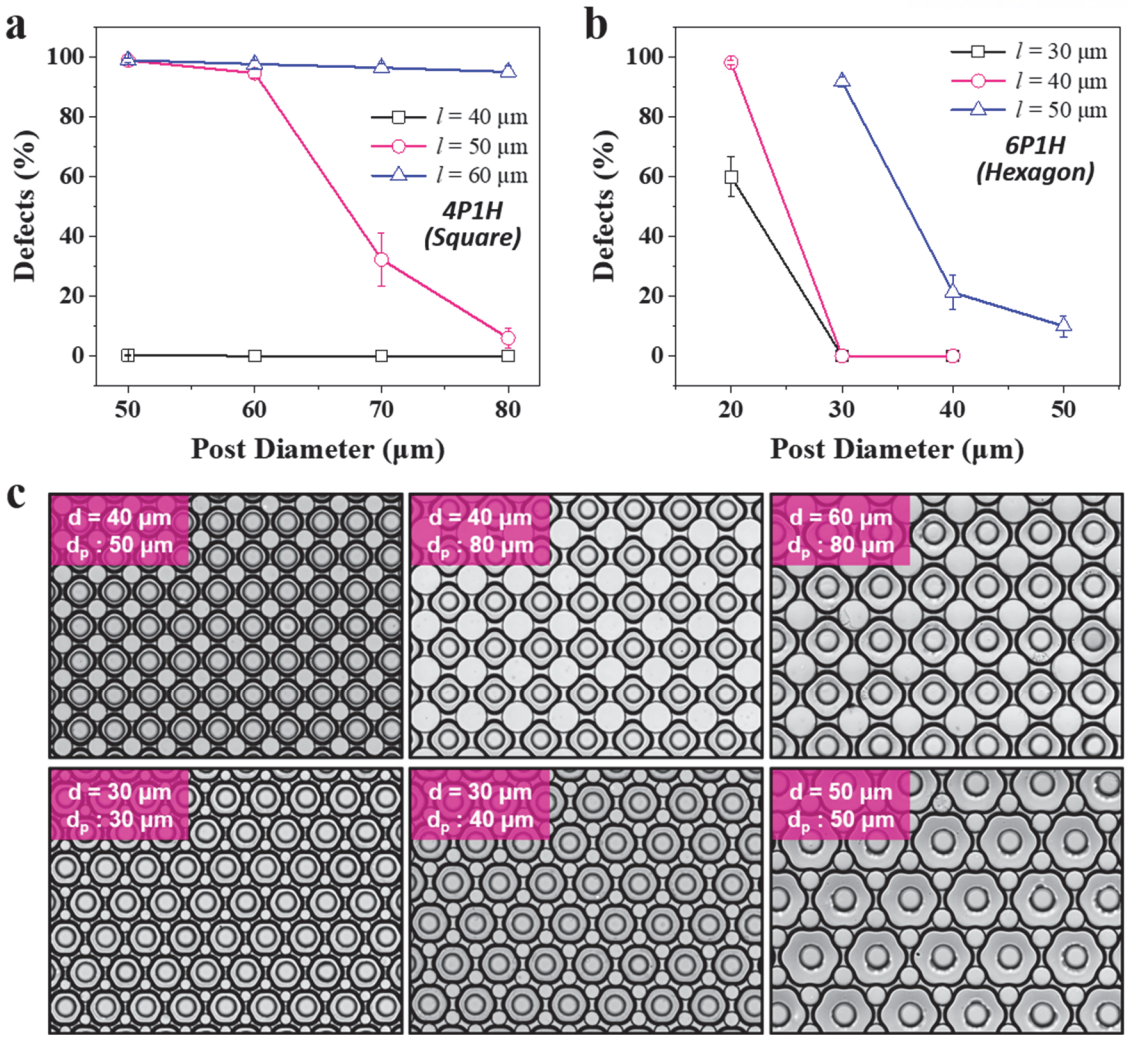

Figure 29. Characterization of defects in liquid films patterned by varying the parameters of through-hole and post arrays. (a) In rectangular arrays, quantification of defects in liquid films in the range of 40 to 60 μm for l and 50 to 80 μm for d. (b) In hexagonal arrays, defect quantification of liquid films in the range of 30 to 50 μm for l and 20 to 50 μm for d. (c) Images of liquid films formation when a 1:12 ratio mixture of hexadecane and hexane is injected into square and hexagonal through-hole and post arrays. Error bars represent the standard deviation over the entire patterned area.

5.4 Solidified films patterning with a high aspect ratio and durability using photoresist

The method of forming solidified films is to use water and particles as in the previously mentioned literature. After injecting a mixture of water and particles into a microfluidic device, as the water

evaporates, the remaining particles are aligned between posts due to the strong surface tension of water, forming micro-/nano scale thin films. Water and particles were used to form solidified films, but photoresists and non-polar organic solvents were used instead to form solidified films (Figure 30). The materials used were SU-8 series negative photoresists and AZ series photoresists. The SU-8 series used in the experiment were SU-8 2005 and SU-8 2010, and these solutions were obtained from Kayaku Advanced Materials. And the AZ series used in the experiment were AZ GXR 601 (14 CP), AZ GXR 601 (46 CP), AZ P4330, AZ 9260, AZ 5214, and AZ nLOF 2035, and these solutions were obtained from AZ Electronic Materials. First, the process of patterning using SU-8 was similar to that of forming liquid films using non-polar organic solvents. When selecting non-polar organic solvents in the previous section, there were several solutions such as hexane, octane, toluene, petroleum ether, ethyl ether, and pentane that could form liquid films while being mixed with hexadecane. However, when photoresists were used, toluene was the only solution that met the above conditions. Comparing the solids content of SU-8 photoresists, 2000.5 was 14.3%, 2002 was 20%, 2005 was 45%, 2007 was 52.5%, 2010 was 58%, and 2015 was 63.45%. The higher the solids content, the stronger the stickiness, which is advantageous to form solidified films. However, a solution with a higher solid content than SU-8 2010 had a handling problem because it was very sticky, and it was difficult to make a mixed solution with an accurate ratio. In addition, a solution with a lower solids content than SU-8 2005 was not suitable for forming desired hard films because of its lower viscosity. In this experiment, SU-8 2005 and SU-8 2010 were selected and used to form solidified films. SU-8 negative photoresists and toluene were mixed in a 1:9 ratio and injected into the post-hole arrays membrane. Then, the toluene evaporated, and the air trapped in the hole pushed out the SU-8 negative photoresists, forming liquid films with an air/SU-8 photoresist/air interface. To induce complete evaporation of the residual toluene and hardening of the SU-8 negative photoresists, the membrane was placed in an 85 ℃ oven for 1 hour. After that, patterning was performed using AZ series photoresists as well, and the process was the same as that of patterning using SU-8 negative photoresists. AZ photoresists and toluene were mixed in a ratio of 1:9 and injected into the post-hole arrays membrane. Then, the toluene evaporated, and the air trapped in the hole pushed out the AZ photoresists, forming liquid films with an air/AZ photoresist/air interface. To induce complete evaporation of the residual toluene and hardening of the AZ photoresists, the membrane was placed in an 85 °C oven for 1 hour. In AZ series photoresists, viscosity had a great influence on the degree to which solidified films were formed. Figure 30 shows that among the AZ series photoresists used, AZ P4330 and AZ 9260 have 127 cSt and 500 cSt, respectively, and patterning using these two photoresists was the most stable, and it was inferred that the factor was high viscosity. At the air/AZ photoresist/air interface, even when the air was in contact with each other, the films could

withstand without bursting due to the high viscosity of the photoresist, and the solidified films once formed remained in their state even after a few days.

SU-8 2000	% Solids	Dinsity (g/ml)	Viscosity (cSt)
2000.5	14.3	2.49	1.07
2002	29	7.5	1.123
2005	45	45	1.164
2007	52.5	140	1.175
2010	58	380	1.187
2015	63.45	1250	1.2

Table 2. The SU-8 2000 series types used in the experiment, and values for % solids, density, and viscosity.

AZ Series	Polarity	Film Thickness (μm)	Viscosity (cSt)
AZ GXR 601 (14 CP)	Positive	0.8 ~ 1.5	13.95
AZ GXR 601 (46 CP)	Positive	2 ~ 4.5	43
AZ P4330	Positive	3 ~ 5	127
AZ 9260	Positive	5 ~ 20	500
AZ 5214	Image Reversal	1 ~ 2	24
AZ nLOF 2035	Negative (Cross-linking)	3 ~ 5	75

Table 3. AZ series types used in the experiment and values for polarity, film thickness, and viscosity of each.

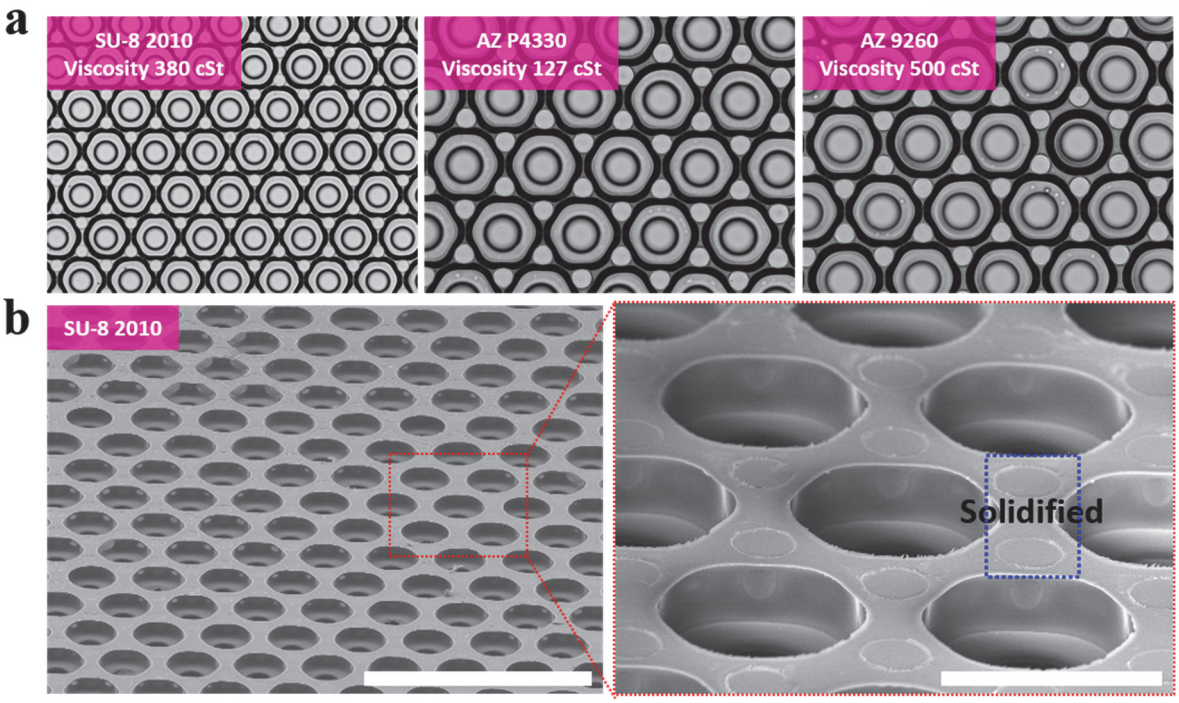

Figure 30. Patterning organic films with a high aspect ratio and durability using photoresist and toluene. (a) Images obtained by patterning solidified films using negative and positive photoresists. The toluene was completely evaporated by injecting a mixture of photoresist and toluene mixed in a ratio of 1:9 to the membrane and then placing it in an oven at 65 °C for 1 hour. Due to the high viscosity of the photoresist, sticky solidified films were patterned. (b) SEM images of the solidified films patterned with SU-8 2010. The scale bars are 400 μm (left) and 100 μm (right).

Chapter 6. Conclusion

We successfully demonstrated that SMFTCEs with high conductivity and excellent durability can be fabricated in a high-throughput manner using TGF technology. This platform, which has through-holes and posts, induces evaporation of liquid and facilitates film formation, and it presents the potential to increase throughput by allowing the device to be fabricated at a large scale. SMFTCEs with high electrical properties were developed with TGF technology using AgNWs, and exhibited outstanding performance in durability, especially through bending tests. SMFTCEs based on the aligned AgNWs network exhibited a sheet resistance of up to 14 Ω/sq. It maintained a constant conductivity regardless of the curvature of the patterned substrates and proved to be an optoelectronic device in a network of well-aligned grids with a transmittance of 80-92%. Mechanical flexibility was demonstrated through bending tests, showing only 6-12% change in sheet resistance even after 10,000 bending cycles of 3 mm curvature. Also, through the fabrication of PFTCEs using PEDOT:PSS showing similar trends to SMFTCEs in curved patterning or bending tests, the potential of application to various materials using TGF technology was also shown. In addition, to overcome the conventional method of patterning FTCEs based on water, liquid film patterns were also fabricated using oil and non-polar organic solvents. To secure the long-term stability of the liquid films, oil that hardly evaporated was injected, and non-polar organic solvents were used to slightly induce evaporation of the oil. The durability of the liquid films in this work was demonstrated by not only being able to control the thickness of the liquid films by adjusting the ratio of organic solvents but also maintaining thin films with a thickness of fewer than 1 μm for up to a day. The high flexural strength of liquid films produced by dissolving the oil in organic solvents was demonstrated, and if a conductive material is applied to liquid films, it is expected to exhibit higher electrical properties than solid conductive grids due to its high aspect ratio. For highly efficient FTCEs, conductive grids patterned in simple steps not only exhibit high transmittance, conductivity, and flexural rigidity but also demonstrate through patterning of various solutions, broadening a new field of view for next-generation functional optoelectronics. In this context, the direct patterning of various materials based on TGF technology can be fabricated with high repeatability in a facile, cost-effective, and high-throughput manner. By replacing the previous ITO-based electrodes, it presents a promising strategy for next-generation electronic applications such as displays, touch screens, and wearable electronics.

REFERENCES

1. Kataoka, D. E.; Troian, S. M., Patterning liquid flow on the microscopic scale. *Nature* **1999,** *402* (6763), 794-797.
2. Ferraro, P.; Coppola, S.; Grilli, S.; Paturzo, M.; Vespini, V., Dispensing nano–pico droplets and liquid patterning by pyroelectrodynamic shooting. *Nature nanotechnology* **2010,** *5* (6), 429-435.
3. Huang, Z.; Su, M.; Yang, Q.; Li, Z.; Chen, S.; Li, Y.; Zhou, X.; Li, F.; Song, Y., A general patterning approach by manipulating the evolution of two-dimensional liquid foams. *Nature communications* **2017,** *8* (1), 1-9.
4. Witomska, S.; Leydecker, T.; Ciesielski, A.; Samorì, P., Production and patterning of liquid phase–exfoliated 2D sheets for applications in optoelectronics. *Advanced Functional Materials* **2019,** *29* (22), 1901126.
5. Ma, B.; Xu, C.; Chi, J.; Chen, J.; Zhao, C.; Liu, H., A versatile approach for direct patterning of liquid metal using magnetic field. *Advanced Functional Materials* **2019,** *29* (28), 1901370.
6. Zhang, R.; Redford, S. A.; Ruijgrok, P. V.; Kumar, N.; Mozaffari, A.; Zemsky, S.; Dinner, A. R.; Vitelli, V.; Bryant, Z.; Gardel, M. L., Spatiotemporal control of liquid crystal structure and dynamics through activity patterning. *Nature Materials* **2021**, 1-8.
7. Park, K. S.; Baek, J.; Park, Y.; Lee, L.; Lee, Y. E.; Kang, Y.; Sung, M. M., Inkjet-Assisted Nanotransfer Printing for Large-Scale Integrated Nanopatterns of Various Single-Crystal Organic Materials. *Adv Mater* **2016,** *28* (15), 2874-80.
8. Park, K. S.; Lee, K. S.; Baek, J.; Lee, L.; Son, B. H.; Koo Lee, Y. E.; Ahn, Y. H.; Park, W. I.; Kang, Y.; Sung, M. M., Observation of Charge Separation and Space-Charge Region in Single-Crystal P3HT/C60 Heterojunction Nanowires. *Angew Chem Int Ed Engl* **2016,** *55* (35), 10273-7.
9. Lone, S.; Zhang, J. M.; Vakarelski, I. U.; Li, E. Q.; Thoroddsen, S. T., Evaporative Lithography in Open Microfluidic Channel Networks. *Langmuir* **2017,** *33* (11), 2861-2871.
10. Bae, J.; Lee, J.; Zhou, Q.; Kim, T., Micro-/Nanofluidics for Liquid-Mediated Patterning of Hybrid-Scale Material Structures. *Advanced Materials* **2019,** *31* (20), 1804953.
11. Miralles, V.; Selva, B.; Cantat, I.; Jullien, M.-C., Foam drainage control using thermocapillary stress in a two-dimensional microchamber. *Physical review letters* **2014,** *112* (23), 238302.
12. Moulton, D.; Pelesko, J., Reverse draining of a magnetic soap film. *Physical Review E* **2010,** *81* (4), 046320.
13. Binks, B. P.; Horozov, T. S., Aqueous foams stabilized solely by silica nanoparticles. *Angewandte Chemie International Edition* **2005,** *44* (24), 3722-3725.
14. Blijdenstein, T.; De Groot, P.; Stoyanov, S., On the link between foam coarsening and surface rheology: why hydrophobins are so different. *Soft Matter* **2010,** *6* (8), 1799-1808.
15. Fameau, A. L.; Saint-Jalmes, A.; Cousin, F.; Houinsou Houssou, B.; Novales, B.; Navailles, L.; Nallet, F.; Gaillard, C.; Boué, F.; Douliez, J. P., Smart foams: switching reversibly between ultrastable and unstable foams. *Angewandte Chemie International Edition* **2011,** *50* (36), 8264-8269.

16. Sear, R. P.; Chung, S.-W.; Markovich, G.; Gelbart, W. M.; Heath, J. R., Spontaneous patterning of quantum dots at the air-water interface. *Physical Review E* **1999,** *59* (6), R6255.
17. Fan, D.; Jia, X.; Tang, P.; Hao, J.; Liu, T., Self-Patterning of Hydrophobic Materials into Highly Ordered Honeycomb Nanostructures at the Air/Water Interface. *Angewandte Chemie International Edition* **2007,** *46* (18), 3342-3345.
18. Shin, J.; Ko, J.; Jeong, S.; Won, P.; Lee, Y.; Kim, J.; Hong, S.; Jeon, N. L.; Ko, S. H., Monolithic digital patterning of polydimethylsiloxane with successive laser pyrolysis. *Nature Materials* **2021,** *20* (1), 100-107.
19. Zhang, B.; Meng, F.; Feng, J.; Wang, J.; Wu, Y.; Jiang, L., Manipulation of Colloidal Particles in Three Dimensions via Microfluid Engineering. *Adv Mater* **2018,** *30* (22), e1707291.
20. Park, D.; Kang, M.; Choi, J. W.; Paik, S. M.; Ko, J.; Lee, S.; Lee, Y.; Son, K.; Ha, J.; Choi, M.; Park, W.; Kim, H. Y.; Jeon, N. L., Microstructure guided multi-scale liquid patterning on an open surface. *Lab Chip* **2018,** *18* (14), 2013-2022.
21. Bae, J.; Lee, K.; Seo, S.; Park, J. G.; Zhou, Q.; Kim, T., Controlled open-cell two-dimensional liquid foam generation for micro-and nanoscale patterning of materials. *Nature communications* **2019,** *10* (1), 1-9.
22. Yamamoto, D.; Nakajima, C.; Shioi, A.; Krafft, M. P.; Yoshikawa, K., The evolution of spatial ordering of oil drops fast spreading on a water surface. *Nature communications* **2015,** *6* (1), 1-6.
23. Keiser, L.; Bense, H.; Colinet, P.; Bico, J.; Reyssat, E., Marangoni bursting: evaporation-induced emulsification of binary mixtures on a liquid layer. *Physical review letters* **2017,** *118* (7), 074504.
24. Minas, C.; Carnelli, D.; Tervoort, E.; Studart, A. R., 3D printing of emulsions and foams into hierarchical porous ceramics. *Advanced Materials* **2016,** *28* (45), 9993-9999.
25. Zhu, P.; Kong, T.; Tang, X.; Wang, L., Well-defined porous membranes for robust omniphobic surfaces via microfluidic emulsion templating. *Nat Commun* **2017,** *8*, 15823.
26. Li, Z.; Huang, Z.; Li, F.; Su, M.; Li, H.; Zhang, Z.; Wang, Y.; Song, Y., Domino Patterning of Water and Oil Induced by Emulsion Breaking. *ACS Appl Mater Interfaces* **2019,** *11* (19), 17960-17967.
27. Gao, H.; Feng, J.; Zhang, B.; Xiao, C.; Wu, Y.; Kan, X.; Su, B.; Wang, Z.; Hu, W.; Sun, Y.; Jiang, L.; Heeger, A. J., Capillary-Bridge Mediated Assembly of Conjugated Polymer Arrays toward Organic Photodetectors. *Advanced Functional Materials* **2017,** *27* (34).
28. Deng, W.; Lu, B.; Mao, J.; Lu, Z.; Zhang, X.; Jie, J., Precise Positioning of Organic Semiconductor Single Crystals with Two-Component Aligned Structure through 3D Wettability-Induced Sequential Assembly. *ACS Appl Mater Interfaces* **2019,** *11* (39), 36205-36212.
29. Deng, W.; Jie, J.; Xu, X.; Xiao, Y.; Lu, B.; Zhang, X.; Zhang, X., A Microchannel-Confined Crystallization Strategy Enables Blade Coating of Perovskite Single Crystal Arrays for Device Integration. *Adv Mater* **2020,** *32* (16), e1908340.
30. Zhang, X.; Mao, J.; Deng, W.; Xu, X.; Huang, L.; Zhang, X.; Lee, S. T.; Jie, J., Precise Patterning of Laterally Stacked Organic Microbelt Heterojunction Arrays by Surface-Energy-Controlled Stepwise Crystallization for Ambipolar Organic Field-Effect Transistors. *Adv Mater* **2018**, e1800187.

31. Zhao, X.; Liu, T.; Liu, H.; Wang, S.; Li, X.; Zhang, Y.; Hou, X.; Liu, Z.; Shi, W.; Dennis, T. J. S., Organic Single-Crystalline p-n Heterojunctions for High-Performance Ambipolar Field-Effect Transistors and Broadband Photodetectors. *ACS Appl Mater Interfaces* **2018,** *10* (49), 42715-42722.
32. Feng, J.; Jiang, X.; Yan, X.; Wu, Y.; Su, B.; Fu, H.; Yao, J.; Jiang, L., "Capillary-Bridge Lithography" for Patterning Organic Crystals toward Mode-Tunable Microlaser Arrays. *Adv Mater* **2017,** *29* (1).
33. Zhong, Z.; Woo, K.; Kim, I.; Kim, H.; Ko, P.; Kang, D.; Kwon, S.; Kim, H.; Youn, H.; Moon, J., Defect-Free, Highly Uniform Washable Transparent Electrodes Induced by Selective Light Irradiation. *Small* **2018,** *14* (21), 1800676.
34. Kang, M.-G.; Kim, M.-S.; Kim, J.; Guo, L. J., Organic Solar Cells Using Nanoimprinted Transparent Metal Electrodes. *Advanced Materials* **2008,** *20* (23), 4408-4413.
35. Zhao, G.; Kim, S. M.; Lee, S. G.; Bae, T. S.; Mun, C.; Lee, S.; Yu, H.; Lee, G. H.; Lee, H. S.; Song, M., Bendable solar cells from stable, flexible, and transparent conducting electrodes fabricated using a nitrogen-doped ultrathin copper film. *Advanced Functional Materials* **2016,** *26* (23), 4180-4191.
36. Zhao, G.; Wang, W.; Bae, T.-S.; Lee, S.-G.; Mun, C.; Lee, S.; Yu, H.; Lee, G.-H.; Song, M.; Yun, J., Stable ultrathin partially oxidized copper film electrode for highly efficient flexible solar cells. *Nature communications* **2015,** *6* (1), 1-8.
37. Kim, J.-G.; Lee, J.-E.; Jo, S. M.; Chin, B. D.; Baek, J.-Y.; Ahn, K.-J.; Kang, S. J.; Kim, H.-K., Room temperature processed high mobility W-doped In 2 O 3 electrodes coated via in-line arc plasma ion plating for flexible OLEDs and quantum dots LEDs. *Scientific reports* **2018,** *8* (1), 1-13.
38. Madaria, A. R.; Kumar, A.; Zhou, C., Large scale, highly conductive and patterned transparent films of silver nanowires on arbitrary substrates and their application in touch screens. *Nanotechnology* **2011,** *22* (24), 245201.
39. Chu, H. C.; Chang, Y. C.; Lin, Y.; Chang, S. H.; Chang, W. C.; Li, G. A.; Tuan, H. Y., Spray-Deposited Large-Area Copper Nanowire Transparent Conductive Electrodes and Their Uses for Touch Screen Applications. *ACS Appl Mater Interfaces* **2016,** *8* (20), 13009-17.
40. Zhou, Q.; Park, J. G.; Kim, K. N.; Thokchom, A. K.; Bae, J.; Baik, J. M.; Kim, T., Transparent-flexible-multimodal triboelectric nanogenerators for mechanical energy harvesting and self-powered sensor applications. *Nano Energy* **2018,** *48*, 471-480.
41. Li, L.; Zhang, B.; Zou, B.; Xie, R.; Zhang, T.; Li, S.; Zheng, B.; Wu, J.; Weng, J.; Zhang, W., Fabrication of flexible transparent electrode with enhanced conductivity from hierarchical metal grids. *ACS applied materials & interfaces* **2017,** *9* (45), 39110-39115.
42. Kang, S.; Kim, T.; Cho, S.; Lee, Y.; Choe, A.; Walker, B.; Ko, S. J.; Kim, J. Y.; Ko, H., Capillary Printing of Highly Aligned Silver Nanowire Transparent Electrodes for High-Performance Optoelectronic Devices. *Nano Lett* **2015,** *15* (12), 7933-42.
43. Schneider, J.; Rohner, P.; Thureja, D.; Schmid, M.; Galliker, P.; Poulikakos, D., Electrohydrodynamic NanoDrip Printing of High Aspect Ratio Metal Grid Transparent Electrodes. *Advanced Functional Materials* **2016,** *26* (6), 833-840.
44. Lee, H. B.; Jin, W.-Y.; Ovhal, M. M.; Kumar, N.; Kang, J.-W., Flexible transparent conducting electrodes based on metal meshes for organic optoelectronic device applications: a review. *Journal of Materials Chemistry C* **2019,** *7* (5), 1087-1110.

45. Joe, D. J.; Kim, S.; Park, J. H.; Park, D. Y.; Lee, H. E.; Im, T. H.; Choi, I.; Ruoff, R. S.; Lee, K. J., Laser–material interactions for flexible applications. *Advanced Materials* **2017,** *29* (26), 1606586.
46. Yu, X.; Qi, D.; Zhang, Q.; Paeng, D.; Han, X.; Wang, A.; Huang, D.; Wang, L.; Zhang, Z.; Chen, S., Fabrication of flexible transparent Ag square-shaped mesh electrode by top-flat nanosecond laser ablation. *Optics letters* **2020,** *45* (4), 901-904.
47. Su, M.; Qin, F.; Zhang, Z.; Chen, B.; Pan, Q.; Huang, Z.; Cai, Z.; Zhao, Z.; Hu, X.; Derome, D.; Carmeliet, J.; Song, Y., Non-Lithography Hydrodynamic Printing of Micro/Nanostructures on Curved Surfaces. *Angew Chem Int Ed Engl* **2020,** *59* (34), 14234-14240.
48. Rao, K.; Gupta, R.; Kulkarni, G. U., Fabrication of large area, high-performance, transparent conducting electrodes using a spontaneously formed crackle network as template. *Advanced Materials Interfaces* **2014,** *1* (6), 1400090.
49. Hu, L.; Hecht, D.; Grüner, G., Percolation in transparent and conducting carbon nanotube networks. *Nano letters* **2004,** *4* (12), 2513-2517.
50. Wu, Z.; Chen, Z.; Du, X.; Logan, J. M.; Sippel, J.; Nikolou, M.; Kamaras, K.; Reynolds, J. R.; Tanner, D. B.; Hebard, A. F., Transparent, conductive carbon nanotube films. *Science* **2004,** *305* (5688), 1273-1276.
51. Ye, S.; Rathmell, A. R.; Chen, Z.; Stewart, I. E.; Wiley, B. J., Metal nanowire networks: the next generation of transparent conductors. *Advanced materials* **2014,** *26* (39), 6670-6687.
52. Deng, B.; Hsu, P. C.; Chen, G.; Chandrashekar, B. N.; Liao, L.; Ayitimuda, Z.; Wu, J.; Guo, Y.; Lin, L.; Zhou, Y.; Aisijiang, M.; Xie, Q.; Cui, Y.; Liu, Z.; Peng, H., Roll-to-Roll Encapsulation of Metal Nanowires between Graphene and Plastic Substrate for High-Performance Flexible Transparent Electrodes. *Nano Lett* **2015,** *15* (6), 4206-13.
53. Lee, J.-Y.; Connor, S. T.; Cui, Y.; Peumans, P., Solution-processed metal nanowire mesh transparent electrodes. *Nano letters* **2008,** *8* (2), 689-692.
54. Bae, S.; Kim, H.; Lee, Y.; Xu, X.; Park, J. S.; Zheng, Y.; Balakrishnan, J.; Lei, T.; Kim, H. R.; Song, Y. I.; Kim, Y. J.; Kim, K. S.; Ozyilmaz, B.; Ahn, J. H.; Hong, B. H.; Iijima, S., Roll-to-roll production of 30-inch graphene films for transparent electrodes. *Nat Nanotechnol* **2010,** *5* (8), 574-8.
55. Choi, Y.-Y.; Kang, S. J.; Kim, H.-K.; Choi, W. M.; Na, S.-I., Multilayer graphene films as transparent electrodes for organic photovoltaic devices. *Solar Energy Materials and Solar Cells* **2012,** *96*, 281-285.
56. Kim, K. S.; Zhao, Y.; Jang, H.; Lee, S. Y.; Kim, J. M.; Kim, K. S.; Ahn, J. H.; Kim, P.; Choi, J. Y.; Hong, B. H., Large-scale pattern growth of graphene films for stretchable transparent electrodes. *Nature* **2009,** *457* (7230), 706-10.
57. Tokuno, T.; Nogi, M.; Karakawa, M.; Jiu, J.; Nge, T. T.; Aso, Y.; Suganuma, K., Fabrication of silver nanowire transparent electrodes at room temperature. *Nano Research* **2011,** *4* (12), 1215-1222.
58. Hu, L.; Kim, H. S.; Lee, J.-Y.; Peumans, P.; Cui, Y., Scalable Coating and Properties of Transparent, Flexible, Silver Nanowire Electrodes. *ACS Nano* **2010,** *4* (5), 2955-2963.
59. Rathmell, A. R.; Bergin, S. M.; Hua, Y. L.; Li, Z. Y.; Wiley, B. J., The growth mechanism of copper nanowires and their properties in flexible, transparent conducting films. *Advanced materials* **2010,** *22* (32), 3558-3563.

60. Rathmell, A. R.; Wiley, B. J., The synthesis and coating of long, thin copper nanowires to make flexible, transparent conducting films on plastic substrates. *Advanced Materials* **2011,** *23* (41), 4798-4803.
61. Zhong, Z.; Lee, H.; Kang, D.; Kwon, S.; Choi, Y. M.; Kim, I.; Kim, K. Y.; Lee, Y.; Woo, K.; Moon, J., Continuous Patterning of Copper Nanowire-Based Transparent Conducting Electrodes for Use in Flexible Electronic Applications. *ACS Nano* **2016,** *10* (8), 7847-54.
62. Nam, V. B.; Lee, D., Copper Nanowires and Their Applications for Flexible, Transparent Conducting Films: A Review. *Nanomaterials (Basel)* **2016,** *6* (3).
63. Khan, A.; Huang, Y. T.; Miyasaka, T.; Ikegami, M.; Feng, S. P.; Li, W. D., Solution-Processed Transparent Nickel-Mesh Counter Electrode with in-Situ Electrodeposited Platinum Nanoparticles for Full-Plastic Bifacial Dye-Sensitized Solar Cells. *ACS Appl Mater Interfaces* **2017,** *9* (9), 8083-8091.
64. Hecht, D. S.; Hu, L.; Irvin, G., Emerging transparent electrodes based on thin films of carbon nanotubes, graphene, and metallic nanostructures. *Adv Mater* **2011,** *23* (13), 1482-513.
65. Lyons, P. E.; De, S.; Elias, J.; Schamel, M.; Philippe, L.; Bellew, A. T.; Boland, J. J.; Coleman, J. N., High-performance transparent conductors from networks of gold nanowires. *The Journal of Physical Chemistry Letters* **2011,** *2* (24), 3058-3062.
66. Wang, Z.; Yang, X.; Yang, Z.; Guo, W.; Lin, L.; Li, N.; Jiang, E.; Zhang, J.; Yan, B.; Ye, J., Metal-enhanced adsorption of high-density polyelectrolyte nucleation-inducing seed layer for highly conductive transparent ultrathin metal films. *Frontiers in Materials* **2019,** *6*, 18.
67. Zhong, Z.; Lee, S.-H.; Ko, P.; Kwon, S.; Youn, H.; Seok, J. Y.; Woo, K., Control of thermal deformation with photonic sintering of ultrathin nanowire transparent electrodes. *Nanoscale* **2020,** *12* (4), 2366-2373.
68. Huang, J.; Lu, Y.; Wu, W.; Li, J.; Zhang, X.; Zhu, C.; Yang, Y.; Xu, F.; Song, W., Amino-functionalized sub-40 nm ultrathin Ag/ZnO transparent electrodes for flexible polymer dispersed liquid crystal devices. *Journal of Applied Physics* **2017,** *122* (19), 195302.
69. Zhong, Z.; Woo, K.; Kim, I.; Hwang, H.; Kwon, S.; Choi, Y.-M.; Lee, Y.; Lee, T.-M.; Kim, K.; Moon, J., Roll-to-roll-compatible, flexible, transparent electrodes based on self-nanoembedded Cu nanowires using intense pulsed light irradiation. *Nanoscale* **2016,** *8* (16), 8995-9003.
70. Sticker, D.; Rothbauer, M.; Lechner, S.; Hehenberger, M. T.; Ertl, P., Multi-layered, membrane-integrated microfluidics based on replica molding of a thiol-ene epoxy thermoset for organ-on-a-chip applications. *Lab Chip* **2015,** *15* (24), 4542-54.
71. Wang, Z.; Volinsky, A. A.; Gallant, N. D., Crosslinking effect on polydimethylsiloxane elastic modulus measured by custom-built compression instrument. *Journal of Applied Polymer Science* **2014,** *131* (22).
72. Geczy, R.; Sticker, D.; Bovet, N.; Häfeli, U. O.; Kutter, J. P., Chloroform compatible, thiol-ene based replica molded micro chemical devices as an alternative to glass microfluidic chips. *Lab on a Chip* **2019,** *19* (5), 798-806.
73. Decrop, D.; Pardon, G.; Brancato, L.; Kil, D.; Zandi Shafagh, R.; Kokalj, T.; Haraldsson, T.; Puers, R.; van der Wijngaart, W.; Lammertyn, J., Single-Step Imprinting of Femtoliter Microwell Arrays Allows Digital Bioassays with Attomolar Limit of Detection. *ACS Appl Mater Interfaces* **2017,** *9* (12), 10418-10426.

74. Bae, J.; Ju, J.; Kim, D.; Kim, T., Double-Sided Microwells with a Stepped Through-Hole Membrane for High-Throughput Microbial Assays. *Anal Chem* **2020,** *92* (14), 9501-9510.
75. Bae, J.; Chae, Y.; Park, J. G.; Wu, R.; Ju, J.; Kim, T., Direct Single-Step Printing of Conductive Grids on Curved Surfaces Using Template-Guided Foaming. *ACS Appl Mater Interfaces* **2021,** *13* (16), 19168-19175.
76. Paeng, D.; Yoo, J. H.; Yeo, J.; Lee, D.; Kim, E.; Ko, S. H.; Grigoropoulos, C. P., Low-cost facile fabrication of flexible transparent copper electrodes by nanosecond laser ablation. *Advanced Materials* **2015,** *27* (17), 2762-2767.
77. Li, J.; Qin, Q. H.; Shah, A.; Ras, R. H.; Tian, X.; Jokinen, V., Oil droplet self-transportation on oleophobic surfaces. *Science advances* **2016,** *2* (6), e1600148.
78. Tahk, D.; Paik, S.-M.; Lim, J.; Bang, S.; Oh, S.; Ryu, H.; Jeon, N. L., Rapid large area fabrication of multiscale through-hole membranes. *Lab on a Chip* **2017,** *17* (10), 1817-1825.
79. Yao, J. H.; Elder, K. R.; Guo, H.; Grant, M., Theory and simulation of Ostwald ripening. *Phys Rev B Condens Matter* **1993,** *47* (21), 14110-14125.
80. Cai, S.; Bhushan, B., Meniscus and viscous forces during separation of hydrophilic and hydrophobic surfaces with liquid-mediated contacts. *Materials Science and Engineering: R: Reports* **2008,** *61* (1-6), 78-106.

Acknowledgments

First of all, I sincerely appreciate my advisor, Prof. Taesung Kim. He passionately helped me in determining the direction of my research and leading my research and gave me advice on not only my career path but also a wise life. He deeply inspired me by thinking and acting as a researcher. Thanks to him, I was able to grow as a better researcher, and I wish him good health and happiness anytime, anywhere. Also, I appreciate the committee members of my dissertation, Prof. Taesung Kim, Prof. Jaesung Jang, Prof. Hoon-Eui Jeong at UNIST for allowing their valuable time and knowledgeable comments.

I would like to give my appreciation to the members of our lab, MicroFluidics & NanoMechatronics (μFNM) lab at UNIST. Juyeol Bae, who was my senior in the lab and taught me about research attitude and skills, helped me a lot in the field of liquid-mediated patterning, and he was always kind to me, and we spent a lot of time in the lab meaningfully. Jun Gyu Park, who is planning to graduate from a doctoral program, was motivated by his honesty and sincerity, and I respect him as a good researcher. Janghyun Ju, who spent a lot of time with me both inside and outside the lab and now working as a researcher at the company, always gave me passionate advice when I needed help not only in research but also in career-related areas, and we had a meaningful time as good friends. Sangjin Seo, who conducted research with a logical approach, always studied positively and was happy to join me when I needed a discussion. I also thank Yeonghoon Jeong and Dongjun Kim. They not only happily shared administrative duties with me without hesitation but were also good friends. Our laboratory's postdoctoral researcher Dr. Ronghui Wu, her research attitude and ability always inspire me. Dongwoo Seo, who joined our laboratory as a doctoral student, and Hwisu Jeon, who joined as an intern, shared a short time, but their bright and passionate energy convinced me that they could continue as good researchers. I also appreciate the alumni of our lab, Prof. Qitao Zhou, Dr. Dogyeong Ha, Dr. Jongwan Lee, who have supported me a lot since my freshman days and even now. Most importantly, I deeply appreciate all former and current lab members who have had passionate discussions with each other without hesitation. I am convinced that this is the greatest strength of our laboratory and the driving force that develops into an outstanding research community. Additionally, I also thank the staff in the administrative office, Mrs. Kyoungyoung Lim.

I would like to appreciate to my former advisor, Young-Soo Sohn at Daegu Catholic University (DCU), who taught me the basics of my biomedical engineering major and gave me advice in conducting research. And I would also like to thank my former colleagues and friends at DCU.

Lastly, I deeply grateful to my family, Guho Chae, Mihyang Choi, Youngjun Chae, and Soohyun Chae. Without their love and sacrifice, I would not have been today. First of all, to my family, always stay healthy by my side. You have sacrificed for me and dedicated me more than I could ever imagine. So, I will do my best to repay this unfathomable amount of grace.

I would like to close this acknowledgment by conveying the message to my family, ***"It is the greatest happiness and luck in my life to have a family who always trusts me"***. I love you and thank you.